Stem Cell Reports
Article

OPEN ACCESS

Expansion of Adult Human Pancreatic Tissue Yields Organoids Harboring Progenitor Cells with Endocrine Differentiation Potential

Cindy J.M. Loomans,[1,2,8] Nerys Williams Giuliani,[1,2,8] Jeetindra Balak,[2] Femke Ringnalda,[1] Léon van Gurp,[1] Meritxell Huch,[1,3] Sylvia F. Boj,[1] Toshiro Sato,[4] Lennart Kester,[1] Susana M. Chuva de Sousa Lopes,[5] Matthias S. Roost,[5] Susan Bonner-Weir,[6] Marten A. Engelse,[2] Ton J. Rabelink,[2] Harry Heimberg,[7] Robert G.J. Vries,[1] Alexander van Oudenaarden,[1] Françoise Carlotti,[2] Hans Clevers,[1] and Eelco J.P. de Koning[1,2,*]

[1]Hubrecht Institute/KNAW and University Medical Center Utrecht, 3584 CT Utrecht, the Netherlands
[2]Department of Internal Medicine, Leiden University Medical Center, 2333 ZA Leiden, the Netherlands
[3]Wellcome Trust/Cancer Research UK, Gurdon Institute, Cambridge CB2 1QN, UK
[4]Department of Gastroenterology, Keio University, Tokyo 108-8345, Japan
[5]Department of Anatomy and Embryology, Leiden University Medical Center, 2333 ZA Leiden, the Netherlands
[6]Islet Cell & Regenerative Biology, Joslin Diabetes Center, Boston, MA 02215, USA
[7]Beta Cell Neogenesis (BENE), Vrije Universiteit Brussel, 1050 Brussels, Belgium
[8]Co-first author
*Correspondence: e.koning@hubrecht.eu
https://doi.org/10.1016/j.stemcr.2018.02.005

SUMMARY

Generating an unlimited source of human insulin-producing cells is a prerequisite to advance β cell replacement therapy for diabetes. Here, we describe a 3D culture system that supports the expansion of adult human pancreatic tissue and the generation of a cell subpopulation with progenitor characteristics. These cells display high aldehyde dehydrogenase activity ($ALDH^{hi}$), express pancreatic progenitors markers (*PDX1*, *PTF1A*, *CPA1*, and *MYC*), and can form new organoids in contrast to $ALDH^{lo}$ cells. Interestingly, gene expression profiling revealed that $ALDH^{hi}$ cells are closer to human fetal pancreatic tissue compared with adult pancreatic tissue. Endocrine lineage markers were detected upon *in vitro* differentiation. Engrafted organoids differentiated toward insulin-positive (INS^{+}) cells, and circulating human C-peptide was detected upon glucose challenge 1 month after transplantation. Engrafted $ALDH^{hi}$ cells formed INS^{+} cells. We conclude that adult human pancreatic tissue has potential for expansion into 3D structures harboring progenitor cells with endocrine differentiation potential.

INTRODUCTION

β Cell replacement therapy is an attractive therapy to achieve normoglycemia in patients with diabetes mellitus due to severe β cell failure (Nijhoff et al., 2016; Ricordi et al., 1989). The shortage of organ donors severely limits the number of patients that are eligible for current β cell replacement therapy, i.e., pancreas or islet transplantation. Mature human β cells cannot be expanded *in vitro* without complex dedifferentiation and redifferentiation processes (Russ et al., 2008; Gershengorn et al., 2004). Thus, there is an unmet clinical need to generate insulin-producing cells from alternative cell sources to make this therapy more widely available.

Several types of cells have been studied as possible sources of insulin-producing cells, including human embryonic stem cells (hESCs) and human induced pluripotent stem cells (iPSCs). While the phenotype of these cells has long been characterized by immature maturation (Hrvatin et al., 2014), recently more glucose-responsive cells have been generated from human pluripotent stem cells *in vitro* (Pagliuca et al., 2014; Rezania et al., 2014), but safety remains a major concern for any regenerative strategy using hESCs or iPSCs (Lund et al., 2012; Mummery, 2011). An attractive alternative could be the use of putative progenitor cells from adult human pancreas that give rise to the endocrine lineage. Histological studies of human pancreas indicate that neogenesis of insulin-producing cells is associated with the ductal tree in obesity and pregnancy (Butler et al., 2003, 2010). Other studies have also shown that some insulin-producing cells can be generated from cultured human pancreatic ductal tissue (Bonner-Weir et al., 2000; Yatoh et al., 2007; Lee et al., 2010; Klein et al., 2015). We recently showed that *in silico* analysis of single-cell transcriptome profiles of human adult pancreatic cells using a StemID algorithm predicts a distinct subpopulation of ductal cells with multipotential differentiation potential (Grun et al., 2016). In mice, the existence of postnatal endocrine progenitors within the pancreatic ductal population has become controversial, with lineage-tracing experiments showing contradictory results. Although several studies were able to detect endocrine cells derived from the ductal lineage postnatally or after injury (Inada et al., 2008; Xu et al., 2008; Criscimanna et al., 2011; Al-Hasani et al., 2013), others did not find this (Solar et al., 2009; Kopp et al., 2011; Furuyama et al., 2011).

At present, expansion of human pancreatic cells in a standard, 2D culture system is hampered by the transition of both islet (Russ et al., 2009; Gershengorn et al., 2004) and duct cells (Gao et al., 2003; Seeberger et al., 2006; Todorov et al., 2006) to a mesenchymal cell-like phenotype during passaging. This approach does not provide the natural 3D environment of tissues, and thus important information of cell orientation and polarity for proliferation, growth, and differentiation are lost. In fact, proper alignment and polarization of progenitor cells is known to be required for successful differentiation of fetal pancreatic progenitor cells (Kesavan et al., 2009; Cortijo et al., 2012), and 3D culture of fetal murine pancreatic progenitors can be used to unravel and mimic niches important in pancreas development (Greggio et al., 2013). Thus, it is tempting to hypothesize that 3D culture of adult human pancreatic tissue may provide a microenvironment that enhances expansion and differentiation of pancreatic progenitors.

A Matrigel-based 3D culture system was developed in our institute that yields organoids from stem cells in different organs, with the capacity for long-term expansion and generation of functional differentiated organ-specific cells (Sato et al., 2011; Huch et al., 2013a, 2013b). Single isolated adult mouse pancreatic progenitor cells can be expanded by forming colonies or organoids in a Matrigel-based system (Greggio et al., 2013; Huch et al., 2013a; Jin et al., 2013). We observed that these progenitor cells are derived from the ductal tree, express the stem cell marker leucine-rich repeat containing G protein-coupled receptor 5 (*Lgr5*) in culture and are able to differentiate toward the endocrine lineage (Huch et al., 2013a).

RESULTS

Human Pancreatic Tissue Expands as Budding Organoids

Islet-depleted pancreatic tissue after collagenase digestion was obtained from 35 non-diabetic organ donors (age 53.6 ± 12.1 years and BMI 24.7 ± 4.0 kg/m^2) and one organ donor with a history of type 1 diabetes (age 48 years, BMI 21 kg/m^2). After mechanical dissociation the small clumps of tissue were embedded in Matrigel and supplied with an epidermal growth factor/Noggin/R-spondin-based expansion medium. More than 90% of small pancreatic cell clusters formed budding structures within 3 days (Movie S1), and expanded with a cauliflower-like appearance by day 7 (Figure 1A). Some larger cyst-like structures were present in the organoids (Figure 1A). Organoids could be passaged without macroscopic changes in phenotype (Figure 1B), and maintained in culture for at least 10 passages (Figure 1C). The calculated rate for cell doubling was ~67 hr during passage 0 (P0) (n = 3). Growth rate slightly diminished upon passaging (Figure 1C). The proportion of small budding structures and cyst-like structures varied among donors (Figure S1A). Organoids could also be generated from pancreatic tissue from an organ donor with a history of type 1 diabetes (Figure S1B).

Next, we analyzed the cellular composition of organoids in the expansion phase. At day 7 (P0), 92.3% ± 5.4% of organoid cells were positive for the epithelial marker keratin 19 (KRT19), indicating a ductal phenotype (Figures 1D and 1E). Also at passage 3 (P3), the vast majority of the cells still had a ductal phenotype (87.2% ± 8.4% of organoid cells were KRT19$^+$). No insulin-positive (INS$^+$), glucagon-positive (GCG$^+$), or amylase-positive (AMY$^+$) cells were detected in the organoids at day 7 of the expansion phase (P0) (Figures 1D and 1E). The organoids were organized as KRT19$^+$ cells lining cystic or smaller elongated luminal spaces (Figure 1E). In both early and late passages, cells appeared polarized with positive mucin-1 (MUC1) staining at the luminal side of the KRT19$^+$ epithelial lining (Figure 1E). Although human pancreatic cells in 2D culture systems acquire a mesenchymal cell-like phenotype (Gershengorn et al., 2004; Gao et al., 2003; Seeberger et al., 2006; Todorov et al., 2006; Ouziel-Yahalom et al., 2006), few vimentin-positive cells (<2%) were observed in our organoid cultures at P0 or P3 (Figure 1E). Thus, small adult human pancreatic cell clusters can be expanded and passaged in 3D culture, generating polarized ductal budding structures.

Human Pancreatic Organoids Display Pancreatic Progenitors Clustered toward the Tips of the Budding Structures

Since extensive growth by budding was observed, we determined the proliferative capacity of the budding structures. Quantification showed that 27.3% ± 8.7% of the cells within an organoid were Ki67$^+$ at day 7 of expansion (Figure 2A). Only a few Ki67$^+$ cells were negative for the duct marker KRT19 (1.3% ± 0.8% of Ki67$^+$ cells). Ki67$^+$ cells were mainly observed in tips of buds and were not frequently observed in trunk regions (Figure 2B). Also, budding structures with wide tips and narrow trunks were present in the organoids (Figures 2B and 2C). Labeling with the nucleoside analog 5-ethynyl-2′-deoxyuridine that incorporates into newly synthesized DNA further confirmed the location of the proliferative cells toward the tip region (data not shown).

Based on the configuration of the budding structures, we hypothesized that the tips of the budding structures would be enriched for pancreatic progenitor cells, as has been reported for mouse fetal pancreatic development (Zhou et al., 2008; Shih et al., 2013). Immunostaining of the organoids for the pancreatic progenitor markers pancreatic and duodenal homeobox 1 (PDX1) and SRY (sex-determining region Y) box 9 (SOX9)

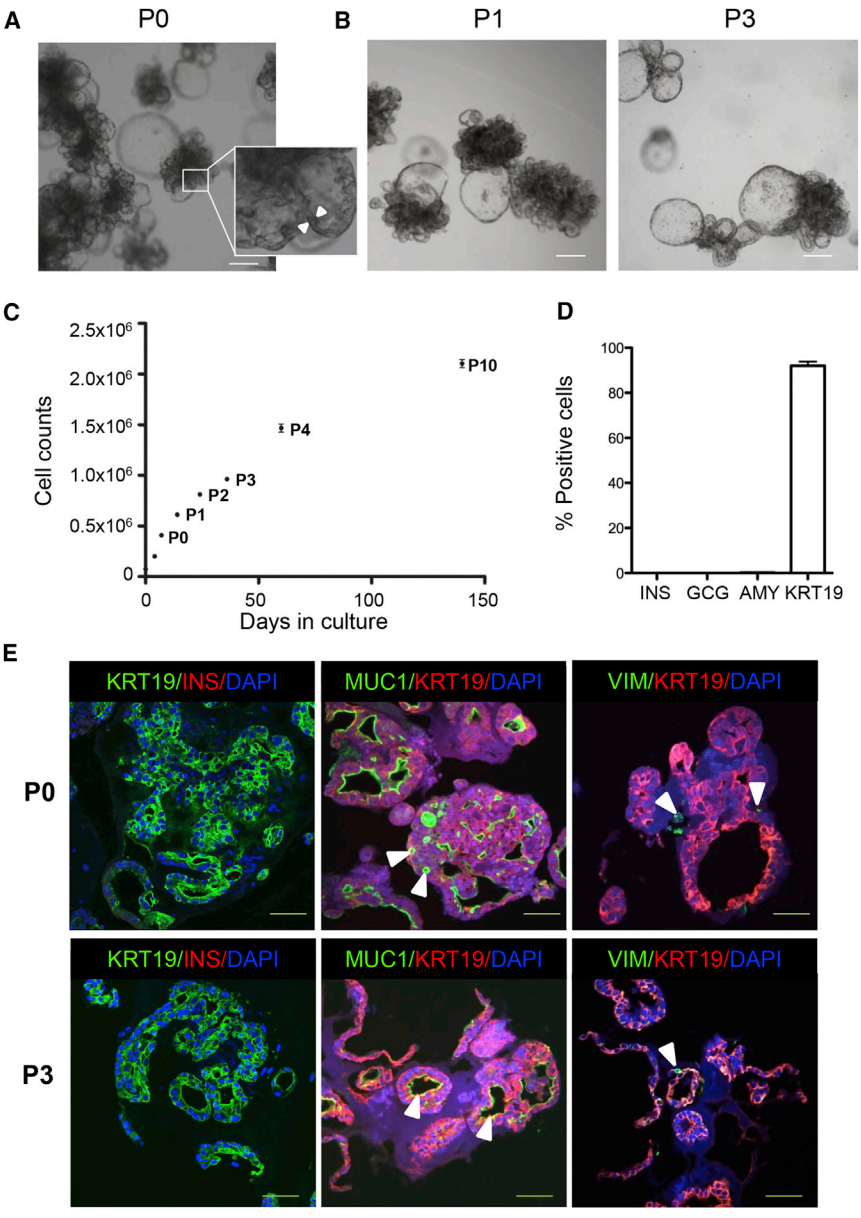

Figure 1. Characterization of Human Pancreatic Organoids during Expansion in a 3D Culture System

(A) Bright-field image of pancreatic organoids (P0), expanded for 7 days in a 3D Matrigel-based culture system, reveals extensive growth with multiple budding structures. Some larger buds have a cyst-like appearance. The insert shows a close-up image of the cell lining (between arrowheads) in a budding structure. Scale bar, 100 μm.

(B) Passaged organoids (P1 and P3 are shown) expanded in similar conditions as P0 (A), also forming budding structures in a cauliflower-like configuration. Scale bar, 100 μm.

(C) Growth curve of pancreatic organoids cultured for 140 days. Cell numbers were counted on days 0, 4, and 7 (P0), and at the end of subsequent passages. Cells in five wells per time point were counted (mean ± SEM). The expansion curve is representative of n = 3 donors.

(D) Quantification of number of cells positive for INS, GCG, AMY, or KRT19 by immunohistochemistry in organoids on day 7 of expansion culture (n = 8 donors; at least 10 organoids/donor were counted; mean ± SEM). DAPI was used as nuclear counterstain.

(E) Non-passaged organoids (P0, upper panels) have similar features compared with passaged organoids (P3, lower panels). Left panels: the majority of the cells are KRT19$^+$ (green), with no INS$^+$ cells (red) detected during the expansion phase. Middle panels: MUC1 (green) staining at the apical cell border indicates polarization of the duct cells. Small lumena are visible within the organoids (arrowheads). Right panels: few vimentin-positive (VIM$^+$) cells (green) are present in the organoids (arrowheads). n = 5 donors; >15 organoids/donor were stained. DAPI was used as nuclear counterstain. Scale bars, 50 μm. See also Figure S1.

(Figure 2B) showed high PDX1 expression in the budding structures of the organoids, particularly in tip regions, while SOX9 was more homogeneously distributed (Figure 2B). *SOX9* and *PDX1* gene expression increased during expansion (Figure S2A). Furthermore, gene expression of *LGR5* increased during this time (Figure S2B), and a subset of cells in budding structures clearly expressed *LGR5* mRNA, as assessed by smFISH (Figure S2C). No neurogenin-3-positive (NEUROG3$^+$) cells were observed in organoids in the expansion phase (Figure 2A). Next, we exposed the organoids to a fluorescent reagent (Aldefluor) that identifies progenitor cells based on their increased aldehyde dehydrogenase activity (ALDH) activity. Pancreatic progenitors with high expression of ALDH1 isoforms have recently been identified in both developing and adult mouse pancreas (Ioannou et al., 2013; Rovira et al., 2010). Cells concentrated in the tips of the budding structures showed high ALDH activity (Figure 2C). The Aldefluor reagent is optimized to detect enzyme activity of ALDH1 isoforms, and we found that ALDH1A1 immunostaining co-localized with both KRT19$^+$ and KRT19$^-$ cells in the tips of the organoid buds, indicating the presence of heterogeneous populations of ALDH1A1$^+$ cells (data not shown). High ALDH activity arose during

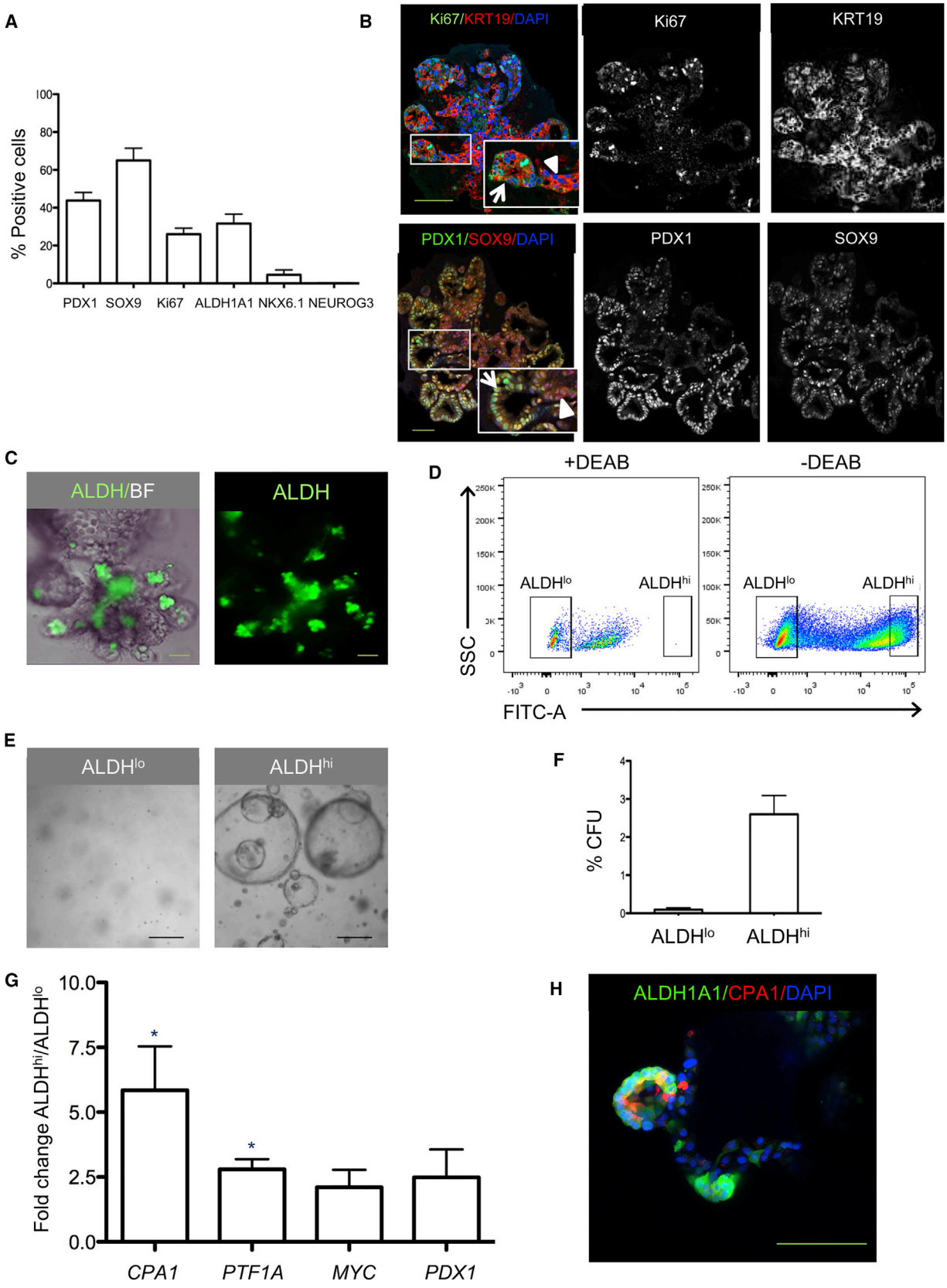

(legend on next page)

organoid culture as no ALDH^{hi} cells were found in the d0 islet-depleted tissue (n = 3; data not shown). *LGR5* gene expression was higher in sorted ALDH^{hi} compared with ALDH^{lo} cells (Figure S2D).

Single ALDH^{hi} Cells Show Progenitor Characteristics

To determine whether ALDH^{hi} cells have characteristics of progenitor cells, organoids were dispersed into single cells, labeled with Aldefluor, and sorted by fluorescence-activated cell sorting (FACS) (ALDH^{lo} cells 34.0% ± 7.4% and ALDH^{hi} cells 25.4% ± 6.0%, n = 5) (Figure 2D). A subpopulation of ALDH^{hi} cells derived from organoids was able to generate small cyst-like colonies in 3D culture (2.2% ± 0.8% of ALDH^{hi} cells), in marked contrast to ALDH^{lo} cells that formed no colonies (Figures 2E, 2F, and S3A). When organoids derived from single-sorted ALDH^{hi} cells were immunostained for ALDH1A1, both ALDH1A1^{+} and ALDH1A1^{-} cells were observed, indicating the generation of a heterogeneous cell population from a single ALDH^{hi} cell (Figure S3B). When these labeled organoids were sorted once more, yet again only ALDH^{hi} cells showed colony-forming potential in 3D culture (data not shown). Interestingly, complex budding structures were not observed when single ALDH^{hi} cells were expanded, which could indicate the requirement of supporting cells for self-assembly into a ductal-tree-like configuration (Figure S3A).

Next, we characterized the ALDH^{hi} cell population for the presence of markers previously described for multipotent progenitor cells in mouse pancreatic organogenesis (Zhou et al., 2008). Gene expression levels of the markers carboxypeptidase A1 (*CPA1*) and pancreas-specific transcription factor, 1a (*PTF1A*) were significantly upregulated in ALDH^{hi} cells compared with the ALDH^{lo} fraction (Figure 2G). Immunoreactivity for CPA1 was found in ALDH1A1^{+} cells in the tips of organoid budding regions, but some ALDH1A1^{+} cells were CPA1^{-} (Figure 2H). Importantly, these ALDH1A1^{+} cells were negative for the acinar cell marker amylase (Figure S3C). Many ALDH1A1^{+} cells in the tips of budding regions buds also co-stained for PDX1 (Figure S3D). Genes that are known to be upregulated in mouse centroacinar (CAC) cells, such as *HES1*, *SOX9*, *SCA1*, *MET*, *NES*, and *HEY1* (Rovira et al., 2010; Kopinke and Murtaugh, 2010), were analyzed in sorted ALDH^{hi} and ALDH^{lo} cells. No upregulation of these markers was present in ALDH^{hi} compared with ALDH^{lo} cells (Figure S3E). HES1^{+} cells were present in expanded organoids after 7 days, but their distribution was not well defined (Figure S3F). Thus, a subpopulation of ALDH^{hi} cells within human pancreatic organoids has colony formation capacity and expresses pancreatic progenitor markers.

Transcriptional Profiling Shows Clustering of ALDH^{hi} Cells from Adult and Fetal Pancreatic Organoids

Since the self-assembly of adult human pancreatic tissue into organoids in our 3D culture system resembles budding structures previously described in pancreatic development, we compared characteristics of organoids derived from adult pancreatic tissue (adult pancreatic organoids) with

Figure 2. Tips of Budding Structures of Pancreatic Organoids Contain Cells with Progenitor Cell Characteristics

(A) Quantification of cells positive for pancreatic progenitor and proliferation markers in organoids on day 7 of expansion culture. Organoids derived from four to six donors were analyzed (at least ten organoids/donor). Data are expressed as mean ± SEM.

(B) Confocal image of pancreatic organoids on day 7 of expansion. Top: organoids were stained for the proliferation marker Ki67 (green) and ductal marker KRT19 (red). Organoid budding structures show a narrow trunk region (arrowhead) and a wider tip region (arrow). Bottom: organoids were stained for SOX9 (red) and PDX1 (green). SOX9^{+} cells were present both in the buds and in the trunk region of the organoids (arrowhead). PDX1^{+} cells (green), which frequently co-expressed SOX9 (yellow), were mainly located in the budding structures with strong staining for PDX1 often observed in cells at the outermost tip regions (arrow). Both overlay and individual channels are depicted. DAPI was used as nuclear counterstain. Scale bars, 100 μm.

(C) Organoids in expansion phase for 7 days were labeled with the Aldefluor fluorescent reagent system, marking progenitor cells characterized by high ALDH activity. Most ALDH^{hi} cells (green) were located in the tips of organoid buds. Scale bar, 50 μm.

(D) FACS analysis of dispersed organoid cells (after 7 days in expansion culture) labeled with Aldefluor with and without the ALDH inhibitor DEAB. The FACS plot shows how ALDH^{hi} cells (i.e., cells that express high ALDH activity) and ALDH^{lo} cells (i.e., cells that express low ALDH activity) are selected. Representative plot from n = 10 donors.

(E) Bright-field images of sorted and expanded single ALDH^{lo} cells (left panel) and ALDH^{hi} cells (right panel) in Matrigel for 14 days. Scale bar, 100 μm.

(F) Proportion of sorted ALDH^{lo} and ALDH^{hi} cells with colony-forming (organoid-forming) potential. Data represent mean ± SEM (n = 3 donors).

(G) Gene expression of *CPA1, PTF1A, MYC*, and *PDX1* in sorted ALDH^{lo} and ALDH^{hi} cells derived from organoids expanded for 7 days. The graph shows the gene expression ratio in ALDH^{hi} to ALDH^{lo} cells for the different markers. Mean ± SEM (n = 3 donors) *p < 0.05.

(H) Whole-mount immunostaining for ALDH1A1 and CPA1 of organoids expanded for 7 days. Confocal images show ALDH1A1^{+} cells (green) and CPA1^{+} cells (red) in the tip of the budding structures. Some cells co-express the two markers. Scale bar, 50 μm.

CFU, colony-forming unit. See also Figures S2 and S3.

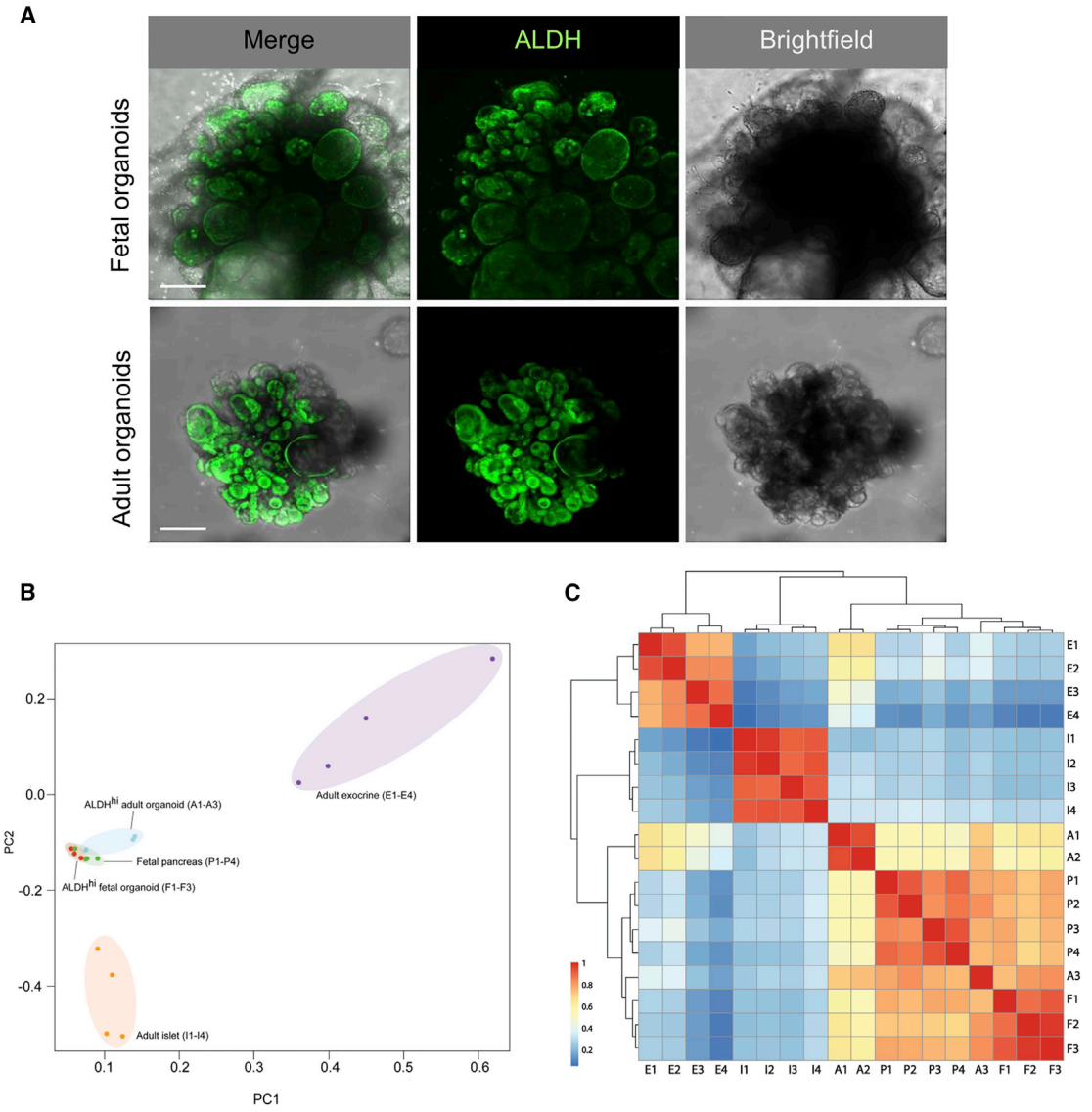

Figure 3. Transcriptional Profiling Shows Clustering of ALDH^{hi} Cells from Adult and Fetal Pancreatic Organoids

(A) Aldefluor labeling of adult and fetal human pancreatic organoids expanded for 7 days. Maximum projection (confocal imaging). Scale bar, 100 μm.

(B) Principal-component analysis for gene expression profiles of the following samples: A1–A3: ALDH^{hi} cells sorted from organoids after 7 days expansion derived from human adult pancreatic tissue (age 50.0 ± 18.7 years, BMI 22.0 ± 4.0 kg/m^2). F1–F3: ALDH^{hi} cells sorted from organoids after 7 days expansion derived from human fetal pancreatic tissue (gestational age: F1 9 weeks, F2 20 weeks, and F3 22 weeks). P1–P4: primary fetal pancreatic tissue (gestational age: P1 9 weeks, P2 18 weeks, P3 14 weeks, and P4 10 weeks). I1–I4: adult human islets (age 34.5 ± 17.3 years, BMI 23.8 ± 4.5 kg/m^2). E1–E4: adult exocrine (islet-depleted) pancreatic tissue (age 63.5 ± 5.7 years, BMI 25.5 ± 3.7 kg/m^2).

(C) Correlation cluster analysis for the gene expression profiles of the samples described in (B).

human fetal pancreatic tissue and organoids derived from this fetal pancreatic tissue (fetal pancreatic organoids). We observed that fetal pancreatic organoids displayed a similar morphology to adult pancreatic organoids under the same culture conditions (Figure 3A). ALDH^{hi} cells were predominantly located in budding structures (Figure 3A). This observation strengthened our hypothesis that ALDH^{hi} cells that are concentrated in tip regions have pancreatic progenitor characteristics. We set out to determine the level of similarity of these putative ALDH^{hi} progenitors isolated from adult pancreatic organoids with ALDH^{hi} cells derived from fetal pancreatic organoids.

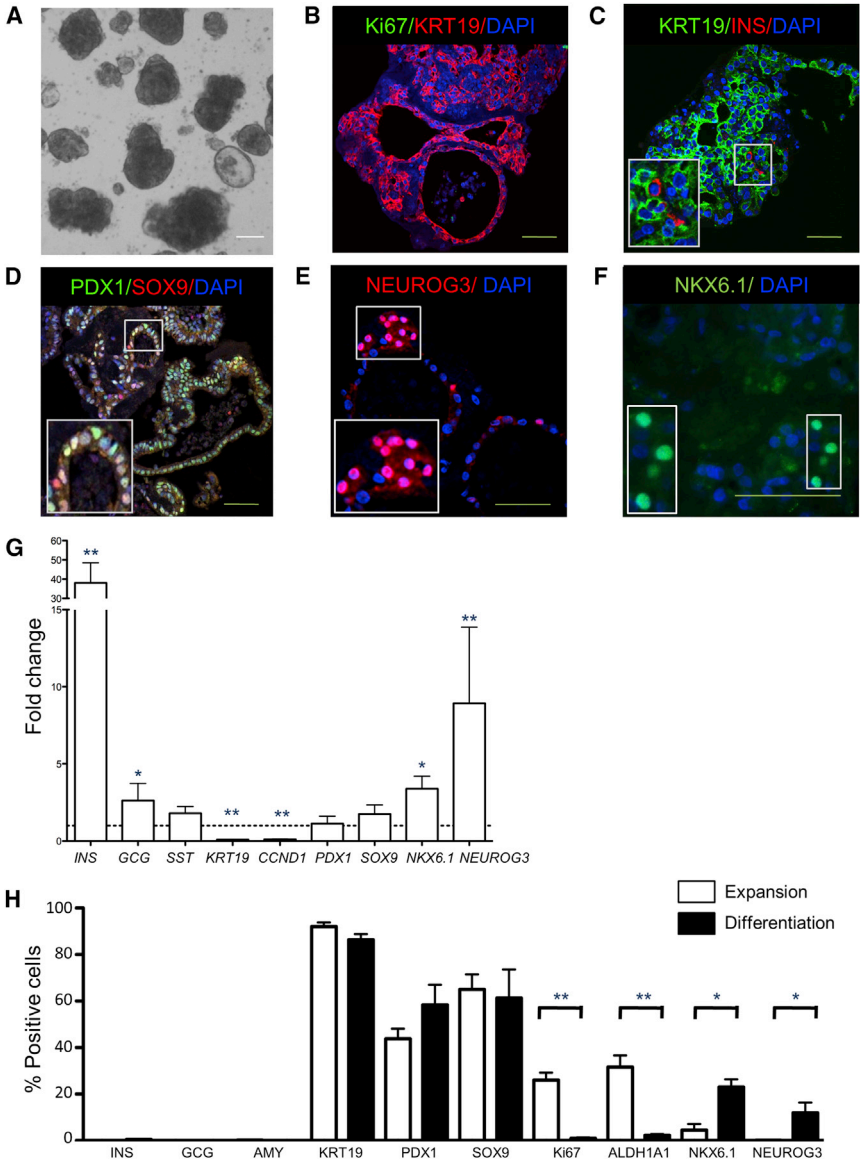

Figure 4. Endocrine Cell Markers in Pancreatic Organoids after 7 Days of *In Vitro* Differentiation

(A) Bright-field image of human pancreatic organoids initially expanded for 7 days followed by differentiation culture for 7 days. DAPI was used as nuclear counterstain. Scale bar, 100 μm.

(B) Confocal image of pancreatic organoids immunostained for Ki67 (green) and KRT19 (red). The majority of cells were KRT19$^+$. No cells were Ki67$^+$. DAPI was used as nuclear counterstain. Scale bar, 50 μm.

(C) Confocal image of pancreatic organoids immunostained for KRT19 (green) and INS (red). Few INS$^+$ (0.52%) cells were present. DAPI was used as nuclear counterstain. Scale bar, 50 μm.

(D) Confocal image of pancreatic progenitor markers PDX1 (green) and SOX9 (red). DAPI was used as nuclear counterstain. Scale bar, 50 μm.

(E) Confocal image of pancreatic progenitor marker NEUROG3 (red). DAPI was used as nuclear counterstain. Scale bar, 50 μm.

(F) Confocal image of pancreatic progenitor marker NKX6.1 (green). DAPI was used as nuclear counterstain. Scale bar, 50 μm.

(G) Gene expression of several markers in organoids on day 7 of differentiation compared with organoids on day 7 of expansion. Gene expression in expansion organoids were set to 1 (dotted line). Mean ± SEM, n = 8 donors. *p < 0.05 and **p < 0.01.

(H) Percentage of cells immunostained for different markers on day 7 of expansion (white bars) compared with day 7 of differentiation (black bars) using confocal images. More than 10 organoids per donor were assessed. Mean ± SEM, n = 4–6 donors. *p < 0.05 and **p < 0.01.

See also Figure S4.

Global gene expression analysis revealed that ALDH^{hi} cells from adult pancreatic organoids are transcriptionally closer to ALDH^{hi} cells isolated from fetal pancreatic organoids than to the adult exocrine tissue they originated from (Figures 3B and 3C). In contrast, ALDH^{hi} cells from fetal pancreatic organoids retained their more primitive identity, clustering closely to fetal pancreatic tissue (Figure 3B). Furthermore, expression levels of the multipotent progenitor markers *CPA1*, *PTF1A*, *PDX1*, and *MYC* in ALDH^{hi} cells from adult pancreatic organoids were comparable with those in ALDH^{hi} cells from organoids derived from fetal pancreas (no significant difference, $p < 0.05$; data not shown).

Pancreatic Organoids Can Differentiate toward an Endocrine Fate *In Vitro*

Since pancreatic organoids expanded from adult human exocrine tissue express progenitor markers during expansion, their differentiation potential was studied using culture conditions reported to differentiate human duct cells (Yatoh et al., 2007; Gao et al., 2005). When P0 organoids were transferred to low attachment plates containing differentiation medium, their budding structure appeared to collapse and a rounded shape was seen after 7 days (Figure 4A). By then, growth had almost completely stopped as indicated by the near absence of Ki67$^+$ cells (0.9% ± 0.4% of total cells; Figures 4B and 4H) and reduced

Cyclin D1 (*CCND1*) gene expression (Figure 4G). Furthermore, the proportion of ALDH1A1$^+$ cells decreased considerably from 27.0% ± 14.5% (P0 expansion day 7) to 1.4% ± 1.3% of total cells (differentiation day 7) (Figure 4H).

A marked increase in insulin gene expression after 7 days of differentiation was observed when compared with the end of the expansion phase (Figure 4G). Despite the considerable increase in insulin gene expression with differentiation, few INS$^+$ cells were observed by immunostaining (0.52% ± 0.22%; Figures 4C and 4H). *GCG* gene expression was only slightly increased between expansion and differentiation (Figure 4G), and no GCG$^+$ cells were present in the differentiation phase (Figure 4H). To exclude the possibility that insulin was taken up from the medium, we confirmed that INS$^+$ cells were also positive for human C-peptide (Figure S4A). No AMY$^+$ cells were observed and the majority of cells remained KRT19$^+$ during differentiation (83.4% ± 14.5% of cells; Figure 4H), even though gene expression of *KRT19* decreased (Figure 4G).

Gene expression of the endocrine progenitor marker *NEUROG3* and β cell marker NKX 6 homeobox 1 (*NKX6.1*) were significantly upregulated during the differentiation phase (Figure 4G). NEUROG3$^+$ cells could also be identified by immunostaining in the "collapsed" organoids (Figures 4E and 4H). In addition, more cells expressed NKX6.1 in the differentiation phase compared with the expansion phase (Figures 4F and 4H). Conversely, no change was found in gene expression of the pancreatic progenitor markers *PDX1* and *SOX9* upon differentiation (Figure 4G) or the number of PDX1$^+$ and SOX9$^+$ cells (Figures 4D and 4H). Thus, upon *in vitro* differentiation, pancreatic progenitors can be directed along the endocrine lineage.

Human Pancreatic Tissue Can Be Cryopreserved without Losing Expansion or Differentiation Capacities

With therapeutic purposes in mind, we explored the possibility of cryopreserving pancreatic tissue before organoid expansion. Freshly retrieved tissue (day 0) was compared with cryopreserved tissue (day 0) from the same donors (n = 4). Growth of organoids with budding structures was observed from both groups (Figure S4B), but the organoids grown from cryopreserved starting material had more cystic appearance than organoids grown from freshly isolated material. When subjected to *in vitro* differentiation, no significant differences in gene expression were found (Figure S4C). Thus, organoids can be grown from cryopreserved primary human adult pancreatic tissue.

Human Pancreatic Organoids Generate Insulin-Producing Cells *In Vivo*

While the *in vitro* differentiation experiments indicated differentiation toward an endocrine lineage based on gene expression analysis, only a few INS$^+$ cells were observed. It is well known that human ESC differentiate into insulin-producing cells after implantation into mice (Kroon et al., 2008). Therefore, we tested the capacity of pancreatic organoids to further differentiate *in vivo* after transplantation under the kidney capsule of immunodeficient mice. One day after transplantation the majority of grafted cells were KRT19$^+$ and no INS$^+$ cells were observed (Figure 5A). However, pancreatic organoids from the same donor 1 month after transplantation showed INS$^+$ cells within the ductal lining (Figure 5B). Organoids derived from each donor (n = 8) were able to generate 1.5% ± 0.2% INS$^+$ cells within the ductal lining (n = 8; Figure 5B). No difference in the proportion of INS$^+$ cells was observed in the hyperglycemic animals (Figure 5C). Production of insulin was confirmed by immunostaining of C-peptide in INS$^+$ cells (CPEP) (Figure S5A). Furthermore, insulin was co-expressed with several functional endocrine markers (PDX1, IAPP, NKX6.1, and SYP) but not with GCG (Figures S5B–S5E). The differentiation phase *in vitro* was necessary for the appearance of INS$^+$ cells as transplantation of organoids 1 week after expansion yielded either no grafts or only large cystic structures with no hormone-positive cells (data not shown).

Human C-peptide could be readily measured in normoglycemic and hyperglycemic mice after a glucose challenge indicating that human insulin was released into the circulation upon a common β cell stimulus (Figure 5D). Basal human C-peptide was also present in normoglycemic mice before the glucose challenge (89.2 ± 59.9 pmol/L, n = 8). Blood glucose of grafted mice did not decrease significantly in either hyperglycemic mice (26.5 ± 3.9 mmol/L at day 0 versus 24.3 ± 3.8 mmol/L at day 30, n = 8) or in the normoglycemic group (8.6 ± 1.3 mmol/L at day 0 versus 6.7 ± 2.4 mmol/L at day 30, n = 8). Thus, graft function was detectable but not sufficient to restore normoglycemia within 1 month after organoid transplantation in hyperglycemic mice.

Sorted ALDH^{hi} cells derived from organoids expanded for 7 days were also differentiated for 1 week *in vitro* and subsequently transplanted under the kidney capsule of normoglycemic immunodeficient mice. After 50 days, retrieved grafts contained both KRT19$^+$ and C-peptide$^+$ cells (Figure 5E).

DISCUSSION

Our data indicate that adult human pancreatic tissue can be expanded as 3D organoids and long-term expansion can be achieved by passaging these pancreatic organoids. Cryopreservation of the pancreatic tissue is possible without losing these characteristics. A subpopulation of

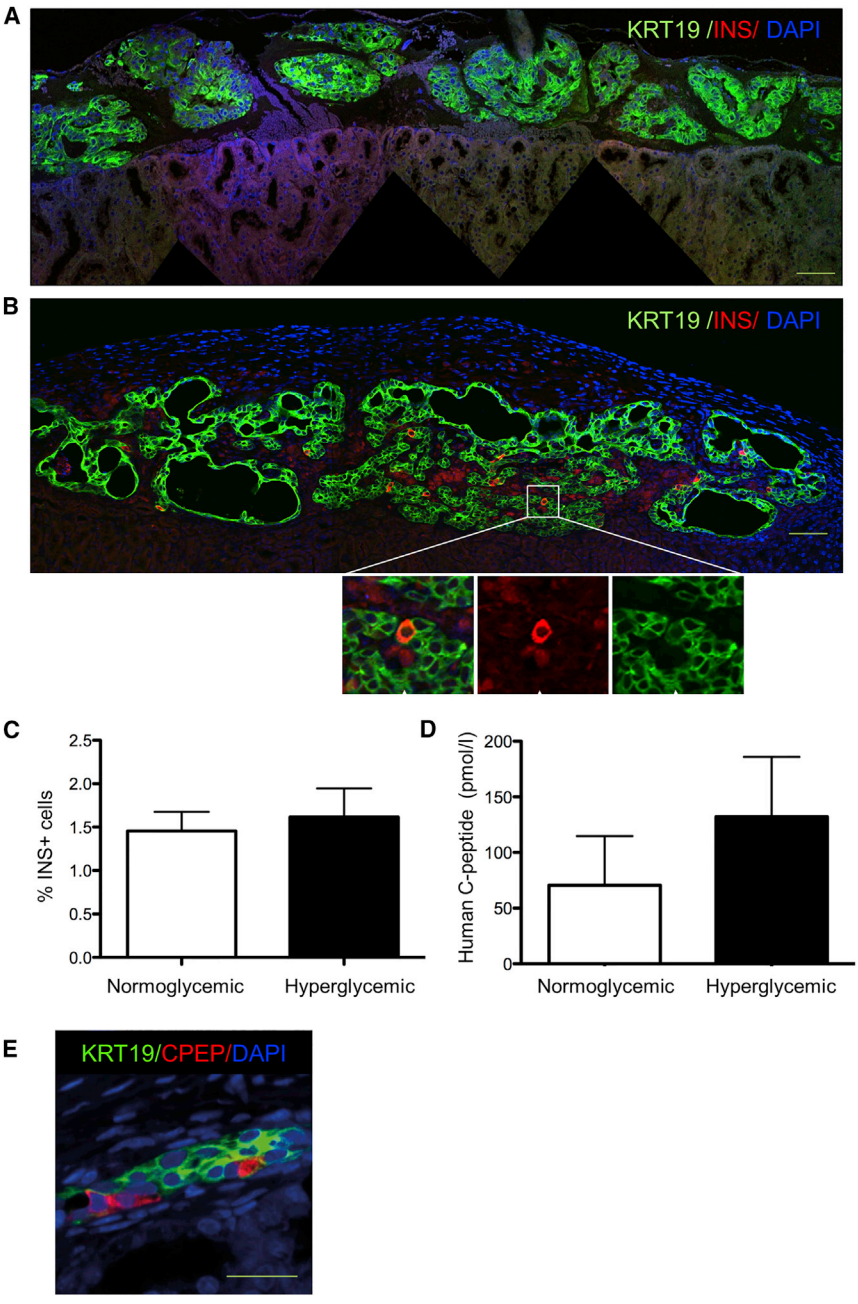

Figure 5. Human Pancreatic Organoids Generate Insulin-Producing Cells *In Vivo*

Grafts composed of *in vitro* differentiated organoids derived from islet-depleted exocrine pancreatic tissue were transplanted under the mouse kidney capsule after 7 days of expansion and 7 days of differentiation.

(A) Day 1 after transplantation. Immunostaining for KRT19 (green) and INS (red). No INS^+ cells are present. DAPI (blue) was used as nuclear counterstain. Scale bar, 50 μm.

(B) Day 30 after transplantation. Transplanted organoids formed a ductal network (KRT19, green) and many INS^+ cells (red) are present within the ductal lining (arrows indicate INS+ cells). DAPI (blue) was used as nuclear counterstain. Scale bar, 50 μm.

(C) Percentage of INS^+ cells in the ductal lining 1 month after transplantation. For each donor, grafts were transplanted in both normoglycemic and hyperglycemic mice, and two mice were transplanted per donor. No significant difference in the number of INS^+ cells between the two groups of mice was found. Mean ± SEM, n = 8 donors.

(D) Human C-peptide concentration after a glucose challenge in mice 1 month after organoid transplantation. Grafts were transplanted in either normoglycemic mice or hyperglycemic mice, and two mice were transplanted per donor. No significant difference in human C-peptide concentration between the two groups of mice was observed. Mean ± SEM, n = 8 donors.

(E) Confocal image of a graft of sorted $ALDH^{hi}$ cells isolated from organoids after expansion for 7 days. The $ALDH^{hi}$ cells were differentiated for 7 days *in vitro* before transplantation under the kidney capsule of normoglycemic mice (n = 3 donors, 1 mouse per donor). The graft was retrieved after 50 days and contained both $KRT19^+$ and $CPEP^+$ cells. Cells co-expressing KRT19 and C-peptide indicate a transition stage from a duct (-like) phenotype to a β (-like) cell phenotype. DAPI (blue) was used as nuclear counterstain. Scale bar, 50 μm.

See also Figure S5.

cells from the organoids have progenitor characteristics and give rise to endocrine cells after transplantation.

Progress to expand human adult pancreatic tissue and thus exploration of its capacity for endocrine cell differentiation has been hampered by epithelial-to-mesenchymal transition in 2D culture systems. The 3D culture system we have developed here provides an environment that allows substantial growth of human pancreatic cells starting from minced tissue. Recently we showed that adult mouse pancreatic organoids can also be expanded using similar culture conditions (Huch et al., 2013a). We and others described Matrigel-based culture methods for expansion of dispersed exocrine cells from adult mouse (Huch et al., 2013a; Jin et al., 2013) and human (Boj et al., 2015) pancreas and for expansion of genetically modified human pancreatic ductal cells (Lee et al., 2013). The striking aspect of our expansion protocol is the self-organization of the tissue into organoids with complex budding structures. These

organoids display a remarkable KRT19^{+} epithelial tree-like structure with apical-basal polarity. This configuration has been shown for mouse embryonic pancreas tissue *in vivo* and *in vitro* (Greggio et al., 2013; Zhou et al., 2008), and is present during human pancreatic organogenesis (Jennings et al., 2013). Similar culture systems enabled the expansion of human intestine and stomach in complex cell configurations, also called organoids, that appear to recapitulate organogenesis and tissue regeneration (Sato et al., 2011; Barker et al., 2010).

During embryogenesis, the tip regions of the expanding ductal trees in the developing pancreas harbor progenitor cells (Zhou et al., 2008; Jennings et al., 2013; Solar et al., 2009); and, in adult human tissue, we predicted, from single-cell transcriptome data, that the progenitor population in human adult pancreatic cells resides among the ductal population (Grun et al., 2016). The morphology of the pancreatic organoids (derived from adult pancreatic tissue) in our study allowed us to search for putative progenitors in the budding structures. ALDH^{hi} cells had differentially high expression of the progenitor markers *PDX1*, *CPA1*, *MYC*, and *PTF1A* (Zhou et al., 2008). In addition, we established organoid culture from human fetal pancreatic tissue. These fetal pancreatic organoids also contained ALDH^{hi} cells in budding structures. Interestingly, transcriptional profiling revealed that ALDH^{hi} cells from adult pancreatic organoids were closer to ALDH^{hi} cells from fetal pancreatic organoids than to adult exocrine tissue (i.e., the islet-depleted tissue before expansion). This indicates a reprogramming of a subset of adult pancreatic cells to a progenitor-like stage.

Organoids expanded from human pancreas and transplanted in immunodeficient mice gave rise to insulin-producing cells after 1 month. The location of the insulin-producing cells in the grafts, i.e., in close proximity of or within the ductal lining, and the increased number of insulin-positive cells after engraftment compared with the initial cell population, support the concept that these cells were newly generated. However, while human C-peptide could be detected in the circulation the number of β cells was not sufficient to restore normoglycemia in diabetic mice 1 month after transplantation. In a recent study by Lee et al. (2013), the authors also showed that a subpopulation of expanded ductal cells could differentiate to insulin-secreting cells using an alternative approach of adenovirus-mediated expression of pro-endocrine factors and co-transplantation with mouse embryonic fibroblasts. In summary, although culture conditions need to be optimized to increase graft efficacy, our study provides a proof-of-concept that this 3D culture system can be used to expand primary human ductal cells that can differentiate to an endocrine fate without the need for genetic modification.

The origin of the ALDH^{hi} cells in our system is unclear. An ALDH^{hi} progenitor cell population has been identified in a subset of adult ductal/CAC cells (Rovira et al., 2010) and in the developing pancreas (Ioannou et al., 2013) of mice, and these cells had the ability to self-renew and to differentiate into both endocrine and exocrine cells.

Notably, several studies have recently attributed a functional role to ALDH1 isoforms during pancreas development in humans (Li et al., 2014), mice (Ostrom et al., 2008), and zebrafish (Matsuda et al., 2013). Our data indicate that the specific culture conditions we developed support this progenitor state. Whether these ALDH^{hi} cells have a CAC origin or not warrants further investigation. At present this question is challenging as there is a lack of markers specific for human adult CACs. In mature murine pancreas, HES1 expression marks terminal ductal or CACs, whereas it identifies MPCs in early embryonic pancreas (until e11.5), and exocrine-restricted progenitors from e13.5 until birth (Kopinke and Murtaugh, 2010). Here, we found that *HES1* was slightly upregulated at the mRNA level in ALDH^{hi} cells, but HES1 protein expression was not restricted to the tips of the budding structures where the majority of ALDH^{hi} cells reside. Finally, the ALDH^{hi} population is heterogeneous, with only a small proportion of cells able to expand *in vitro*. Therefore, additional cell surface markers will be necessary to efficiently enrich and characterize the progenitor subpopulation from this heterogeneous population of ALDH^{hi} cells.

It has been unclear whether an endocrine/multipotent progenitor population exists in the adult human pancreas. Indeed, classical definitions of what constitutes an adult stem cell population are under debate (Clevers, 2015). However, we provide a proof-of-concept for the existence of a ALDH^{hi} population of human pancreatic cells (most likely KRT19^{+} cells) that appears under specific culture conditions, and that has the capacity to differentiate into an endocrine cell phenotype. Aldefluor has been used to detect ALDH^{hi} stem/progenitor cells in multiple tissues (Balber, 2011). Here, we show that this cell population expresses the pancreatic progenitor markers *CPA1*, *PDX1*, *MYC*, and *PTF1A*. Furthermore, the gene expression profile of adult pancreatic ALDH^{hi} population presents a high degree of similarity with fetal pancreatic ALDH^{hi} cells.

Finally, since these cells are derived from the adult human pancreas and, thus, have already committed to a pancreatic fate, differentiation to the β cell lineage may be easier to achieve than differentiation of other adult stem/progenitor cells. In current allogeneic and autologous islet transplantation contaminating non-islet cells from the human pancreas are always co-transplanted with islets into human recipients without adverse effects (Ichii et al., 2008). Therefore, expanded and differentiated adult

human pancreatic cells are likely to be relatively safe compared with embryonic or induced pluripotent cell lines for future β cell replacement therapy programs.

EXPERIMENTAL PROCEDURES

Human Primary Tissue

Adult Pancreatic Tissue

Islet-depleted pancreatic tissue and human islets that could not be used for clinical transplantation were used in the studies according to national laws and if research content was available.

Fetal Pancreatic Tissue

Fetal pancreatic tissue from elective abortions was used after written (parental) informed consent was provided. Collection and use of human fetal tissue for research was approved by the Medical Ethics committee of the LUMC.

Generation of Human and Fetal Pancreatic Organoids

Human adult islet-depleted pancreatic tissue was obtained after human islet isolation procedures. For culture of adult pancreatic organoids, small pieces of exocrine tissue were plated and expanded in Matrigel (BD Biosciences). Human fetal pancreatic tissue was obtained from fetuses with a gestational age of 9, 20, and 22 weeks. For culture of fetal pancreatic organoids, small pieces of human fetal pancreatic tissue were plated and expanded in Matrigel similar to adult pancreatic organoids. A progenitor population within the organoids was identified using the Aldefluor fluorescent reagent system (STEMCELL), which is based on detection of high ALDH activity in progenitor cells. $ALDH^{hi}$ and $ALDH^{lo}$ cell populations were sorted and plated in Matrigel before analysis. Human and fetal pancreatic organoids were analyzed by immunohistochemistry, RNA sequencing, qPCR, and smFISH, For a detailed description see Supplemental Experimental Procedures.

In Vitro and *In Vivo* Differentiation of Human Pancreatic Organoids

After expansion, adult pancreatic organoids were retrieved from the Matrigel and analyzed, cryopreserved in liquid nitrogen, or transferred to a differentiation culture medium (3 mL), characterized by absence of growth factors, in six-well hydrophobic plates (Corning). Organoids were cultured for 7–18 days before analysis or transplantation under the kidney capsule in normoglycemic or hyperglycemic immunodeficient mice. Human C-peptide was measured and grafts were analyzed up to 1 month after transplantation. For a detailed description see Supplemental Experimental Procedures.

ACCESSION NUMBERS

The accession number for the RNA sequencing data reported in this paper is GEO: GSE108854.

SUPPLEMENTAL INFORMATION

Supplemental Information includes Supplemental Experimental Procedures, five figures, two tables, and one movie and can be found with this article online at https://doi.org/10.1016/j.stemcr.2018.02.005.

AUTHOR CONTRIBUTIONS

C.J.M.L. and N.W.G. performed the key experiments and co-wrote the manuscript with E.J.P.d.K., H.C., and F.C. J.B. performed the experiments with fetal pancreatic organoids. F.R. and L.v.G. provided technical assistance. M.H., S.F.B., T.S., H.C., R.G.J.V., and H.H. provided expertise on organoids culture systems and culture of human cells. S.B.-W. provided expertise on human pancreatic duct cells. T.J.R. provided the infrastructure for human pancreatic tissue isolation. L.K. and A.v.O. gave support for the RNA sequencing experiments. S.M.C.d.S.L. and M.S.R. provided human fetal pancreatic tissue. M.A.E. provided human adult pancreatic tissue.

ACKNOWLEDGMENTS

This work was financially supported by the DON foundation, the Dutch Diabetes Research Foundation, the Tjanka Foundation, and the Diabetes Cell Therapy Initiative. We thank Dr. Vrolijk for help with analyses of immunostaining (ImageJ-based data analyses), Yves Heremans (H.H. lab) and Annemieke Tons (Leiden University Medical Center, Leiden) for helping with the NEUROG3 staining, the Hubrecht imaging center for microscope assistance, and Stefan van der Elst (Geijsen lab, Hubrecht Institute, Utrecht) for help with FACS and analysis.

Received: October 24, 2017
Revised: February 8, 2018
Accepted: February 9, 2018
Published: March 13, 2018

REFERENCES

Al-Hasani, K., Pfeifer, A., Courtney, M., Ben-Othman, N., Gjernes, E., Vieira, A., Druelle, N., Avolio, F., Ravassard, P., Leuckx, G., et al. (2013). Adult duct-lining cells can reprogram into beta-like cells able to counter repeated cycles of toxin-induced diabetes. Dev. Cell *26*, 86–100.

Balber, A.E. (2011). Concise review: aldehyde dehydrogenase bright stem and progenitor cell populations from normal tissues: characteristics, activities, and emerging uses in regenerative medicine. Stem Cells *29*, 570–575.

Barker, N., Huch, M., Kujala, P., van de Wetering, M., Snippert, H.J., van Es, J.H., Sato, T., Stange, D.E., Begthel, H., van den Born, M., et al. (2010). Lgr5(+ve) stem cells drive self-renewal in the stomach and build long-lived gastric units in vitro. Cell Stem Cell *6*, 25–36.

Boj, S.F., Hwang, C.I., Baker, L.A., Chio, I.I., Engle, D.D., Corbo, V., Jager, M., Ponz-Sarvise, M., Tiriac, H., Spector, M.S., et al. (2015). Organoid models of human and mouse ductal pancreatic cancer. Cell *160*, 324–338.

Bonner-Weir, S., Taneja, M., Weir, G.C., Tatarkiewicz, K., Song, K.H., Sharma, A., and O'Neil, J.J. (2000). In vitro cultivation of human islets from expanded ductal tissue. Proc. Natl. Acad. Sci. USA *97*, 7999–8004.

Butler, A.E., Janson, J., Bonner-Weir, S., Ritzel, R., Rizza, R.A., and Butler, P.C. (2003). Beta-cell deficit and increased beta-cell

apoptosis in humans with type 2 diabetes. Diabetes *52*, 102–110.

Butler, A.E., Cao-Minh, L., Galasso, R., Rizza, R.A., Corradin, A., Cobelli, C., and Butler, P.C. (2010). Adaptive changes in pancreatic beta cell fractional area and beta cell turnover in human pregnancy. Diabetologia *53*, 2167–2176.

Clevers, H. (2015). STEM CELLS. What is an adult stem cell? Science *350*, 1319–1320.

Cortijo, C., Gouzi, M., Tissir, F., and Grapin-Botton, A. (2012). Planar cell polarity controls pancreatic beta cell differentiation and glucose homeostasis. Cell Rep. *2*, 1593–1606.

Criscimanna, A., Speicher, J.A., Houshmand, G., Shiota, C., Prasadan, K., Ji, B., Logsdon, C.D., Gittes, G.K., and Esni, F. (2011). Duct cells contribute to regeneration of endocrine and acinar cells following pancreatic damage in adult mice. Gastroenterology *141*, 1451–1462, 1462.e1-6.

Furuyama, K., Kawaguchi, Y., Akiyama, H., Horiguchi, M., Kodama, S., Kuhara, T., Hosokawa, S., Elbahrawy, A., Soeda, T., Koizumi, M., et al. (2011). Continuous cell supply from a Sox9-expressing progenitor zone in adult liver, exocrine pancreas and intestine. Nat. Genet. *43*, 34–41.

Gao, R., Ustinov, J., Pulkkinen, M.A., Lundin, K., Korsgren, O., and Otonkoski, T. (2003). Characterization of endocrine progenitor cells and critical factors for their differentiation in human adult pancreatic cell culture. Diabetes *52*, 2007–2015.

Gao, R., Ustinov, J., Korsgren, O., and Otonkoski, T. (2005). In vitro neogenesis of human islets reflects the plasticity of differentiated human pancreatic cells. Diabetologia *48*, 2296–2304.

Gershengorn, M.C., Hardikar, A.A., Wei, C., Geras-Raaka, E., Marcus-Samuels, B., and Raaka, B.M. (2004). Epithelial-to-mesenchymal transition generates proliferative human islet precursor cells. Science *306*, 2261–2264.

Greggio, C., De, F.F., Figueiredo-Larsen, M., Gobaa, S., Ranga, A., Semb, H., Lutolf, M., and Grapin-Botton, A. (2013). Artificial three-dimensional niches deconstruct pancreas development in vitro. Development *140*, 4452–4462.

Grun, D., Muraro, M.J., Boisset, J.C., Wiebrands, K., Lyubimova, A., Dharmadhikari, G., van den Born, M., van, E.J., Jansen, E., Clevers, H., et al. (2016). De novo prediction of stem cell identity using single-cell transcriptome data. Cell Stem Cell *19*, 266–277.

Hrvatin, S., O'Donnell, C.W., Deng, F., Millman, J.R., Pagliuca, F.W., DiIorio, P., Rezania, A., Gifford, D.K., and Melton, D.A. (2014). Differentiated human stem cells resemble fetal, not adult, beta cells. Proc. Natl. Acad. Sci. USA *111*, 3038–3043.

Huch, M., Bonfanti, P., Boj, S.F., Sato, T., Loomans, C.J., van de Wetering, M., Sojoodi, M., Li, V.S., Schuijers, J., Gracanin, A., et al. (2013a). Unlimited in vitro expansion of adult bi-potent pancreas progenitors through the Lgr5/R-spondin axis. EMBO J. *32*, 2708–2721.

Huch, M., Dorrell, C., Boj, S.F., van Es, J.H., Li, V.S., van de Wetering, M., Sato, T., Hamer, K., Sasaki, N., Finegold, M.J., et al. (2013b). In vitro expansion of single Lgr5+ liver stem cells induced by Wnt-driven regeneration. Nature *494*, 247–250.

Ichii, H., Miki, A., Yamamoto, T., Molano, R.D., Barker, S., Mita, A., Rodriguez-Diaz, R., Klein, D., Pastori, R., Alejandro, R., et al. (2008). Characterization of pancreatic ductal cells in human islet preparations. Lab. Invest. *88*, 1167–1177.

Inada, A., Nienaber, C., Katsuta, H., Fujitani, Y., Levine, J., Morita, R., Sharma, A., and Bonner-Weir, S. (2008). Carbonic anhydrase II-positive pancreatic cells are progenitors for both endocrine and exocrine pancreas after birth. Proc. Natl. Acad. Sci. USA *105*, 19915–19919.

Ioannou, M., Serafimidis, I., Arnes, L., Sussel, L., Singh, S., Vasiliou, V., and Gavalas, A. (2013). ALDH1B1 is a potential stem/progenitor marker for multiple pancreas progenitor pools. Dev. Biol. *374*, 153–163.

Jennings, R.E., Berry, A.A., Kirkwood-Wilson, R., Roberts, N.A., Hearn, T., Salisbury, R.J., Blaylock, J., Piper, H.K., and Hanley, N.A. (2013). Development of the human pancreas from foregut to endocrine commitment. Diabetes *62*, 3514–3522.

Jin, L., Feng, T., Shih, H.P., Zerda, R., Luo, A., Hsu, J., Mahdavi, A., Sander, M., Tirrell, D.A., Riggs, A.D., et al. (2013). Colony-forming cells in the adult mouse pancreas are expandable in Matrigel and form endocrine/acinar colonies in laminin hydrogel. Proc. Natl. Acad. Sci. USA *110*, 3907–3912.

Kesavan, G., Sand, F.W., Greiner, T.U., Johansson, J.K., Kobberup, S., Wu, X., Brakebusch, C., and Semb, H. (2009). Cdc42-mediated tubulogenesis controls cell specification. Cell *139*, 791–801.

Klein, D., Alvarez-Cubela, S., Lanzoni, G., Vargas, N., Prabakar, K.R., Boulina, M., Ricordi, C., Inverardi, L., Pastori, R.L., and Dominguez-Bendala, J. (2015). BMP-7 induces adult human pancreatic exocrine-to-endocrine conversion. Diabetes *64*, 4123–4134.

Kopinke, D., and Murtaugh, L.C. (2010). Exocrine-to-endocrine differentiation is detectable only prior to birth in the uninjured mouse pancreas. BMC. Dev. Biol. *10*, 38.

Kopp, J.L., Dubois, C.L., Schaffer, A.E., Hao, E., Shih, H.P., Seymour, P.A., Ma, J., and Sander, M. (2011). Sox9+ ductal cells are multipotent progenitors throughout development but do not produce new endocrine cells in the normal or injured adult pancreas. Development *138*, 653–665.

Kroon, E., Martinson, L.A., Kadoya, K., Bang, A.G., Kelly, O.G., Eliazer, S., Young, H., Richardson, M., Smart, N.G., Cunningham, J., et al. (2008). Pancreatic endoderm derived from human embryonic stem cells generates glucose-responsive insulin-secreting cells in vivo. Nat. Biotechnol. *26*, 443–452.

Lee, J.H., Jo, J., Hardikar, A.A., Periwal, V., and Rane, S.G. (2010). Cdk4 regulates recruitment of quiescent beta-cells and ductal epithelial progenitors to reconstitute beta-cell mass. PLoS One *5*, e8653.

Lee, J., Sugiyama, T., Liu, Y., Wang, J., Gu, X., Lei, J., Markmann, J.F., Miyazaki, S., Miyazaki, J., Szot, G.L., et al. (2013). Expansion and conversion of human pancreatic ductal cells into insulin-secreting endocrine cells. Elife *2*, e00940.

Li, J., Feng, Z.C., Yeung, F.S., Wong, M.R., Oakie, A., Fellows, G.F., Goodyer, C.G., Hess, D.A., and Wang, R. (2014). Aldehyde dehydrogenase 1 activity in the developing human pancreas modulates retinoic acid signalling in mediating islet differentiation and survival. Diabetologia *57*, 754–764.

Lund, R.J., Narva, E., and Lahesmaa, R. (2012). Genetic and epigenetic stability of human pluripotent stem cells. Nat. Rev. Genet. *13*, 732–744.

Matsuda, H., Parsons, M.J., and Leach, S.D. (2013). Aldh1-expressing endocrine progenitor cells regulate secondary islet formation in larval zebrafish pancreas. PLoS One *8*, e74350.

Mummery, C. (2011). Induced pluripotent stem cells – a cautionary note. N. Engl. J. Med. *364*, 2160–2162.

Nijhoff, M.F., Engelse, M.A., Dubbeld, J., Braat, A.E., Ringers, J., Roelen, D.L., van Erkel, A.R., Spijker, H.S., Bouwsma, H., van der Boog, P.J., et al. (2016). Glycemic stability through islet-after-kidney transplantation using an Alemtuzumab-based induction regimen and long-term triple-maintenance immunosuppression. Am. J. Transplant. *16*, 246–253.

Ostrom, M., Loffler, K.A., Edfalk, S., Selander, L., Dahl, U., Ricordi, C., Jeon, J., Correa-Medina, M., Diez, J., and Edlund, H. (2008). Retinoic acid promotes the generation of pancreatic endocrine progenitor cells and their further differentiation into beta-cells. PLoS One *3*, e2841.

Ouziel-Yahalom, L., Zalzman, M., Anker-Kitai, L., Knoller, S., Bar, Y., Glandt, M., Herold, K., and Efrat, S. (2006). Expansion and redifferentiation of adult human pancreatic islet cells. Biochem. Biophys. Res. Commun. *341*, 291–298.

Pagliuca, F.W., Millman, J.R., Gurtler, M., Segel, M., Van, D.A., Ryu, J.H., Peterson, Q.P., Greiner, D., and Melton, D.A. (2014). Generation of functional human pancreatic beta cells in vitro. Cell *159*, 428–439.

Rezania, A., Bruin, J.E., Arora, P., Rubin, A., Batushansky, I., Asadi, A., O'Dwyer, S., Quiskamp, N., Mojibian, M., Albrecht, T., et al. (2014). Reversal of diabetes with insulin-producing cells derived in vitro from human pluripotent stem cells. Nat. Biotechnol. *32*, 1121–1133.

Ricordi, C., Lacy, P.E., and Scharp, D.W. (1989). Automated islet isolation from human pancreas. Diabetes *38* (*Suppl 1*), 140–142.

Rovira, M., Scott, S.G., Liss, A.S., Jensen, J., Thayer, S.P., and Leach, S.D. (2010). Isolation and characterization of centroacinar/terminal ductal progenitor cells in adult mouse pancreas. Proc. Natl. Acad. Sci. USA *107*, 75–80.

Russ, H.A., Bar, Y., Ravassard, P., and Efrat, S. (2008). In vitro proliferation of cells derived from adult human beta-cells revealed by cell-lineage tracing. Diabetes *57*, 1575–1583.

Russ, H.A., Ravassard, P., Kerr-Conte, J., Pattou, F., and Efrat, S. (2009). Epithelial-mesenchymal transition in cells expanded in vitro from lineage-traced adult human pancreatic beta cells. PLoS One *4*, e6417.

Sato, T., Stange, D.E., Ferrante, M., Vries, R.G., van Es, J.H., van den Brink, S., Van Houdt, W.J., Pronk, A., Van, G.J., Siersema, P.D., et al. (2011). Long-term expansion of epithelial organoids from human colon, adenoma, adenocarcinoma, and Barrett's epithelium. Gastroenterology *141*, 1762–1772.

Seeberger, K.L., Dufour, J.M., Shapiro, A.M., Lakey, J.R., Rajotte, R.V., and Korbutt, G.S. (2006). Expansion of mesenchymal stem cells from human pancreatic ductal epithelium. Lab. Invest. *86*, 141–153.

Shih, H.P., Wang, A., and Sander, M. (2013). Pancreas organogenesis: from lineage determination to morphogenesis. Annu. Rev. Cell Dev. Biol. *29*, 81–105.

Solar, M., Cardalda, C., Houbracken, I., Martin, M., Maestro, M.A., De, M.N., Xu, X., Grau, V., Heimberg, H., Bouwens, L., et al. (2009). Pancreatic exocrine duct cells give rise to insulin-producing beta cells during embryogenesis but not after birth. Dev. Cell *17*, 849–860.

Todorov, I., Omori, K., Pascual, M., Rawson, J., Nair, I., Valiente, L., Vuong, T., Matsuda, T., Orr, C., Ferreri, K., et al. (2006). Generation of human islets through expansion and differentiation of non-islet pancreatic cells discarded (pancreatic discard) after islet isolation. Pancreas *32*, 130–138.

Xu, X., D'Hoker, J., Stange, G., Bonne, S., De, L.N., Xiao, X., Van de, C.M., Mellitzer, G., Ling, Z., Pipeleers, D., et al. (2008). Beta cells can be generated from endogenous progenitors in injured adult mouse pancreas. Cell *132*, 197–207.

Yatoh, S., Dodge, R., Akashi, T., Omer, A., Sharma, A., Weir, G.C., and Bonner-Weir, S. (2007). Differentiation of affinity-purified human pancreatic duct cells to beta-cells. Diabetes *56*, 1802–1809.

Zhou, Q., Brown, J., Kanarek, A., Rajagopal, J., and Melton, D.A. (2008). In vivo reprogramming of adult pancreatic exocrine cells to beta-cells. Nature *455*, 627–632.

Stem Cell Reports, Volume *10*

Supplemental Information

Expansion of Adult Human Pancreatic Tissue Yields Organoids Harboring Progenitor Cells with Endocrine Differentiation Potential

Cindy J.M. Loomans, Nerys Williams Giuliani, Jeetindra Balak, Femke Ringnalda, Léon van Gurp, Meritxell Huch, Sylvia F. Boj, Toshiro Sato, Lennart Kester, Susana M. Chuva de Sousa Lopes, Matthias S. Roost, Susan Bonner-Weir, Marten A. Engelse, Ton J. Rabelink, Harry Heimberg, Robert G.J. Vries, Alexander van Oudenaarden, Françoise Carlotti, Hans Clevers, and Eelco J.P. de Koning

Figure S1:

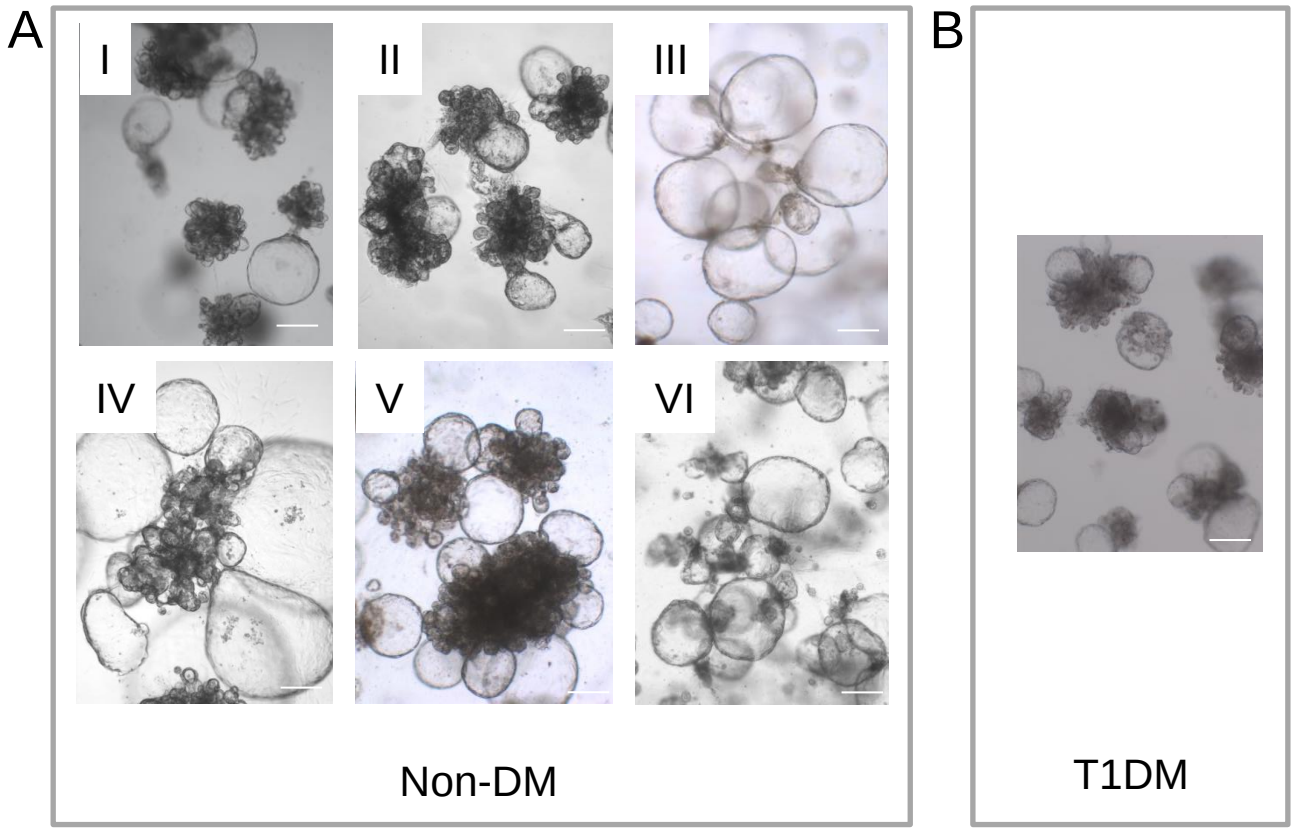

Figure S2:

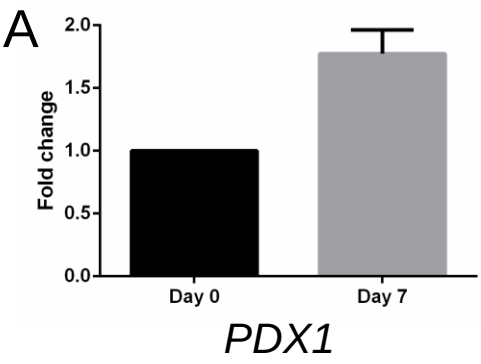
A
Fold change
2.0
1.5
1.0
0.5
0.0
Day 0
Day 7
PDX1

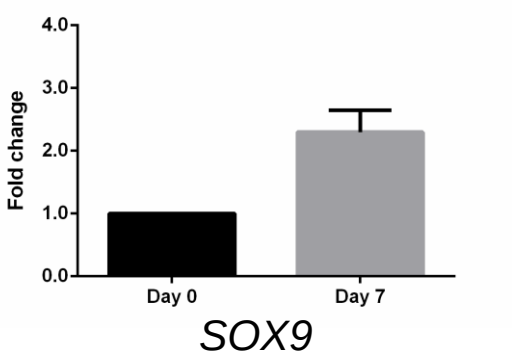
Fold change
4.0
3.0
2.0
1.0
0.0
Day 0
Day 7
SOX9

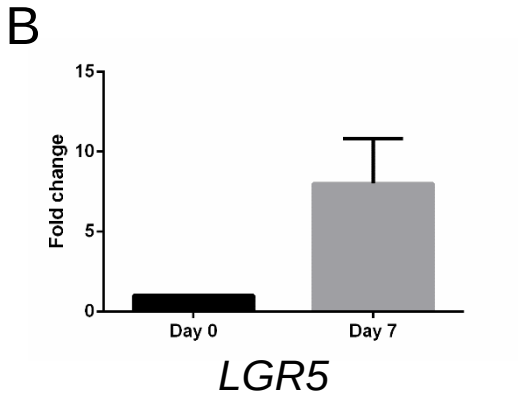
B
Fold change
15
10
5
0
Day 0
Day 7
LGR5

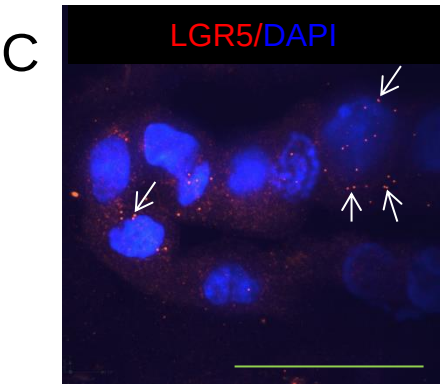
C
LGR5/DAPI

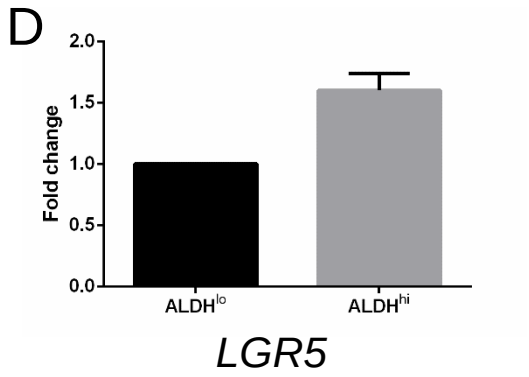
D
Fold change
2.0
1.5
1.0
0.5
0.0
ALDHlo
ALDHhi
LGR5

Figure S3:

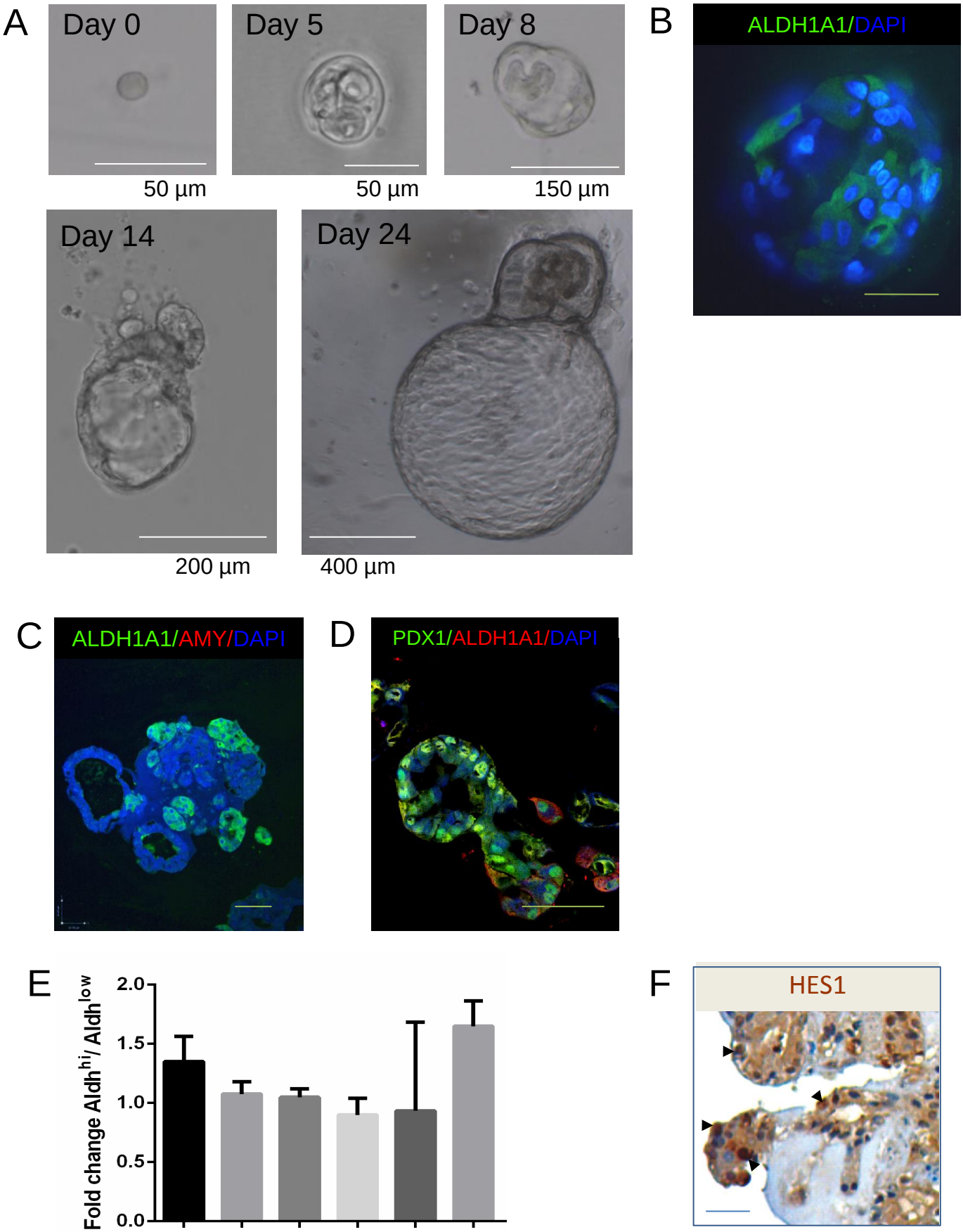
A
Day 0
Day 5
Day 8
50 µm
50 µm
150 µm
Day 14
Day 24
200 µm
400 µm
B
ALDH1A1/DAPI
C
ALDH1A1/AMY/DAPI
D
PDX1/ALDH1A1/DAPI
E
Fold change Aldh^hi/ Aldh^low
2.0
1.5
1.0
0.5
0.0
SOX9
SCA1
MET
NES
HEY1
HES1
F
HES1

Figure S4:

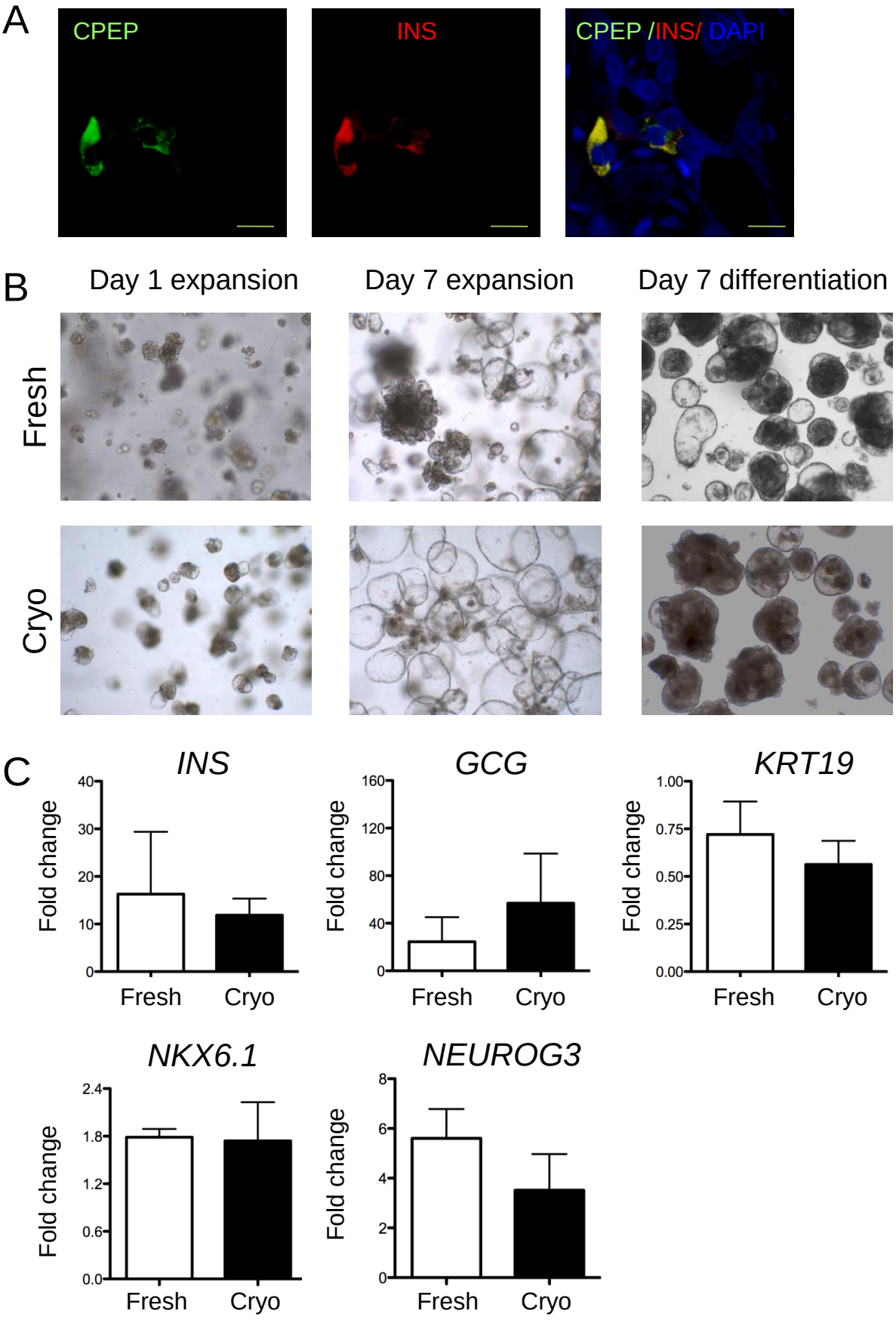
A
CPEP
INS
CPEP /INS/ DAPI
B
Day 1 expansion
Day 7 expansion
Day 7 differentiation
Fresh
Cryo
C
INS
GCG
KRT19
NKX6.1
NEUROG3
Fold change
Fresh
Cryo

Figure S5:

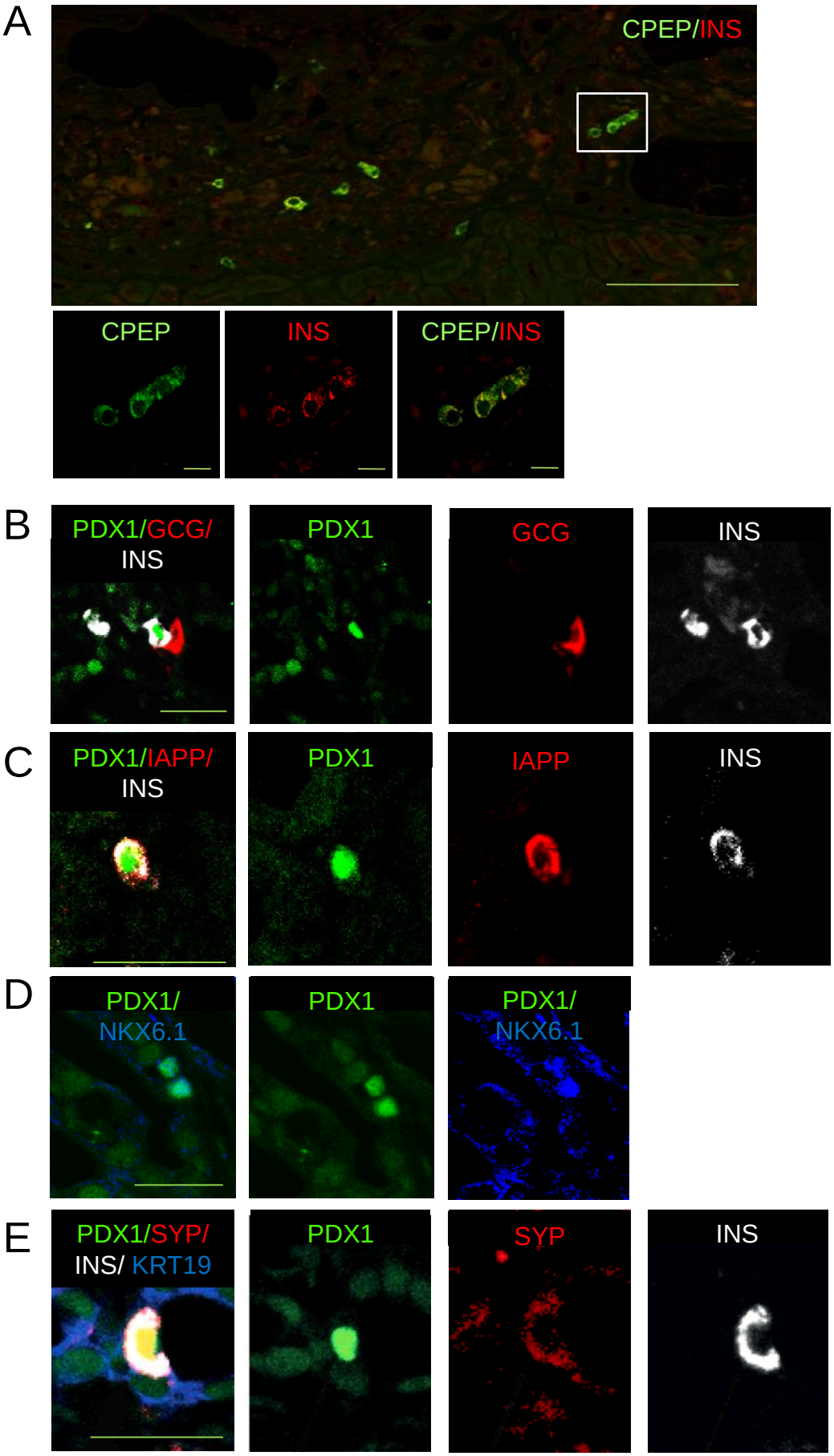
A
CPEP/INS
CPEP
INS
CPEP/INS
B
PDX1/GCG/
INS
PDX1
GCG
INS
C
PDX1/IAPP/
INS
PDX1
IAPP
INS
D
PDX1/
NKX6.1
PDX1
PDX1/
NKX6.1
E
PDX1/SYP/
INS/ KRT19
PDX1
SYP
INS

Table S1: Antibody list

Use	Antibody	Source	Supplier	Dilution	Amplification	Antigen retrieval	Cat. number
Primary	ALDH1A1	goat	R and D systems	1:100	biotin	none	AF5669
Primary	ALDH1A1	rabbit	Abcam	1:100	no	Citrate PH=6.0	ab52492
Primary	AMY2B	mouse	Santa Cruz	1:100	no	Citrate PH=6.0	sc-46657
Primary	C-PEP	mouse	Millipore	1:1000	no	not necessary	05-1109
Primary	CPA1	rabbit	Sigma-Aldrich	1:1000	no	none	HPA021836
Primary	GCG	rabbit	Vector labs	1:200	no	none	VP-G806
Primary	GCG	mouse	Sigma-Aldrich	1:100	no	none	G2654
Primary	HES1	rabbit	Santa Cruz	1:200	no	Citrate PH=6.0	Sc-25392
Primary	IAPP	Mouse	Anne Clark, OCDEM, Oxford	1:1000	no	Citrate PH=6.0	n/a
Primary	INS	Guinea pig	Millipore	1:200	no	none	4011-01F
Primary	Ki67	mouse	Invitrogen	1:200	Biotin	Citrate PH=6.0	18-0192Z
Primary	KRT19	mouse	Dako	1:20	Biotin	Proteinase K	M 0888
Primary	MUCIN1	Armenian hamster	Thermo Scientific	1:200	Biotin	Citrate PH=6.0	HM-1630-R7
Primary	NEUROG3	sheep	R and D systems	1:500	no	Citrate PH=6.0	AF3444
Primary	NKX6.1	rabbit	Sigma Prestige Antibodies	1:500	no	Citrate PH=6.0	HPA036774
Primary	PDX1-Biotinylated	Goat	R and D systems	1:5	Biotin	Citrate PH=6.0	BAF2419
Primary	SOX9	rabbit	Millipore	1:400	no	Citrate PH=6.0	AB5535
Primary	SYP	mouse	Millipore		no	Citrate PH=6.0	MAB5258
Primary	VIM	mouse	Dako	1:100	Biotin	Citrate PH=6.0	M0725
biotinylation	Biotin-anti mouse IgG (H+L)	donkey	Jackson Immuno research labs	1:200	no	n/a	715-065-151
biotinylation	Biotin-anti goat IgG (H+L)	rabbit	Dako	1:200	no	n/a	E 0466
biotinylation	Biotin-anti armenian hamster IgG (H+L)	goat	Affymetrix eBioscience	1:200	n/a	n/a	13-4113
Secondary	Anti rabbit IgG (H+L) Alexafluor 488/568	donkey	Molecular probes	1:200	n/a	n/a	A21206 (488) A10042 (568)
Secondary	Anti goat IgG (H+L) Alexafluor 488	donkey	Molecular probes	1:200	n/a	n/a	A11055
Secondary	Anti mouse IgG (H+L) Alexafluor 488/568	donkey	Molecular probes	1:200	n/a	n/a	A21202 (488) A11061 (568)
Secondary	Tritc-anti guinea pig	donkey	Jackson Immuno research labs	1:400	n/a	n/a	706-025-148
Secondary	Anti sheep IgG (H+L) Alexafluor 568	donkey	Molecular probes	1:200	n/a	n/a	A21099
Secondary	Streptavidin-Alexafluor 488/568	n/a	Molecular probes	1:200	n/a	n/a	S11223 (488) S11226 (568)
Secondary	Anti sheep-HRP	Rabbit	Dako	1:200	n/a	n/a	
Secondary	TSA Plus Cyanine 3/5 System	n/a	Perkin Elmer	1:50	n/a	n/a	NEL744001KT (568) NEL745001KT (647)
F-actin staining	Alexafluor 488 Phalloidin	n/a	Life Technologies	1:1000	n/a	not necessary	A12379
Nuclear staining	DAPI	n/a	Molecular probes	1:10000	n/a	not necessary	D1306

Table S2: Primer sequences

Gene name	Forward (5' →3')	Reverse (5' →3')
INS	GCAGCCTTTGTCAACCAACA	TTCCCCGCACACTAGGTAGAGA
GCG	CAAGGCAGCTGGCAACGT	CTGGTGAATGTGCCCTGTGA
SST	CCCAGACTCCGTCAGTTTCT	ATCATTCTCCGTCTGGTTGG
AMY	GATGGGTTGATATTGCTCTTG	GTATCTTTCCCACCAAGGTC
KRT19	CTACAGCCACTACTACACGAC	CAGAGCCTGTTCCGTCTCAAA
NEUROG3	ACCCTCACTCAAGTCTGTCTG	ATTGGGAGTAGAGCAGATCG
PDX1	CCATGGATGAAGTCTACCAAAGCT	CGTGAGATGTACTTGTTGAATAGGAACT
SOX9	GCCGAGCTCAGCAAGAC	TACTTGTAATCCGGGTGGTC
NKX6.1	CTGGCCTGTACCCCTCATCA	CTTCCCGTCTTTGTCCAACAA
CPA1	TGGTGTTGAGTGTCCTGTTG	GCTCCTTCACCTTCTGTACC
PTF1A	AGGCCCAGAAGGTCATC	AGGGAGGCCATAATCAGG
MYC	TCTCTGAAAGGCTCTCCTTG	CCTGTTGGTGAAGCTAACG
CCD1	GTCCTACTACCGCCTCACAC	AGCAGGGCTTCGATCTG
B2M	GCGCTACTCTCTCTTTCTGG	GCTGGATGACGTGAGTAAAC
GAPDH	GGAAGCTTGTCATCAATGG	TGATGATCTTGAGGCTGTTG

Figure S1. Donor variation in growth of human pancreatic organoids. Related to Figure 1.

A) Brightfield images of pancreatic organoids derived from 6 non-diabetic (non-DM) donors (I –VI) show variability in morphology observed after expansion for 7 days. No clear donor age or BMI dependent differences were observed that relate to variable morphology. Scale bars 50 µm.

B) Brightfield image of pancreatic organoids derived from a donor with Type 1 diabetes mellitus (T1DM), expanded for 7 days. Scale bar 50 µm.

Figure S2. Progenitor markers during expansion and *LGR5* enrichment in ALDH^{hi} cells. Related to Figure 2A-C.

A) Gene expression of *SOX9* and *PDX1* in expansion organoids (d7) compared to islet-depleted starting material (d0). Mean±SEM (n=3 donors).

B) *LGR5* gene expression in expansion organoids (d7) compared to islet-depleted starting material (d0). mean±SEM (n=3 donors).

C) Single molecule fluorescent *in situ* hybridisation (smFISH) of *LGR5* transcripts (red, see arrows) in an organoid budding structure at day 7 of expansion. Scale bar 50µm.

D) *LGR5* gene expression in sorted ALDH^{hi} compared to ALDH^{lo} cells at day 7 of expansion. mean±SEM (n=2 donors).

Figure S3. Characterization of organoids from ALDH^{hi} cells and islet-depleted pancreatic tissue. Related to Figure 2D-H.

A-B) Organoid-forming capacity of sorted ALDH^{hi} cells. A) Representative example of a sorted single ALDH^{hi} cell during expansion. Days of expansion are depicted above the images, the length of scale bars are in the bottom of the pictures. B) Confocal image of a wholemount-stained organoid formed after 2 weeks' expansion culture from a sorted ALDH^{hi} cell. Organoids consists of ALDH1A1^{+} cells (green) as well as ALDH1A1^{-} cells. Scale bar 50µm.

C-F) Gene and protein expression of exocrine and progenitor markers. C) Confocal image of a pancreatic organoid expanded for 7 days. ALDH1A1^{+} cells (green) were located at the tips of budding structures. Immunostaining for amylase was not observed. Scale bar 50µm. D) Confocal image of a

pancreatic organoid expanded for 7 days and immunostained for PDX1 (green) and ALDH1A1 (red). Scale bar 50µm. E) Gene expression for markers, known to be upregulated in mouse centroacinar cells, in sorted $ALDH^{lo}$ and $ALDH^{hi}$ cells derived from organoids expanded for 7 days. The graph shows the gene expression ratio in $ALDH^{hi}$ to $ALDH^{lo}$ cells for the different markers. Mean±SEM (n=2). F) Chromogenic immunostaining of HES1 (brown) in organoids on d7 of expansion. Arrows indicate examples of $HES1^{+}$ cells. Scale bar 50 µM.

Figure S4. Characterization of in vitro differentiated organoids from fresh and cryopreserved pancreatic tissue. Related to Figure 4.

A) Co-localisation of C-peptide with insulin in organoids in vitro. Confocal image of organoids expanded (7 days) and differentiated (7days) *in vitro*, immunostained for human C-peptide (CPEP; green) and insulin (INS; red). All INS^{+} cells in the organoids are also $CPEP^{+}$. DAPI (blue) was used as counterstain. Scale bars 10 µm.

B-C) Cryopreservation of human pancreatic organoids. B) Brightfield images of organoids grown from either freshly retrieved pancreatic tissue (Fresh) (upper panel) or cryopreserved pancreatic tissue (lower panel). Same donors were used to test characteristics (n=4). Representative pictures are shown from day 1 and day 7 expansion and from differentiation cultures (day 7). C) Gene expression profiles of organoids expanded from cryopreserved and fresh pancreatic tissue. Fold change in gene expression between differentiation and expansion conditions was calculated for organoids expanded from fresh and cryopreserved material (mean±SEM, n=4). No significant difference in gene expression was detected between fresh and cryopreserved organoids.

Figure S5. Endocrine markers in grafts of human pancreatic organoids. Related to Figure 5.

A) Immunostaining for C-peptide (CPEP; green) and insulin (INS; red) in grafts of pancreatic organoids, shows that all INS^{+} cells are also $CPEP^{+}$. Scale bar 100 µm. The bottom pictures show confocal images of the insert with co-localisation of C-peptide and insulin. DAPI (blue) was used as counterstain. Scale bars 10 µm.

(B-E) Confocal images from a graft of human pancreatic organoids. (B) PDX1 (green) co-localised with insulin (white), whereas these markers were not detected in GCG^+ cells (red); (C-E) PDX1 (green) also co-localised with IAPP (red), NKX6.1 (blue), and SYP (red). Scale bars 50 μM.

Supplemental movie S1. Formation of budding structures from human islet-depleted adult pancreatic tissue

Time-lapse imaging shows the formation of budding structures from human islet-depleted pancreatic tissue. Imaging was started at day 1 and images were taken for 2.5 days at a rate of 1 image per hour.

Supplemental Table S1: Antibodies used in this study. Related to Figure 1,2,4,5.

Supplemental Table S2: Primer sets used in this study. Related to Figure 2 and 4.

Human adult pancreatic tissue

Human islets were isolated according to a modified Ricordi method by the human islet isolation unit at the Leiden University Medical Center (LUMC). The islet-depleted tissue remaining after islet isolation was used in the studies within one day of islet isolation and the human islets were used within several days of islet isolation (after at least one day culture). CMRL-1066 medium (Cellgro) supplemented with 10% human serum (Blood bank LUMC, Leiden) and 1% penicillin/streptomycin (Invitrogen) was used to culture islet-depleted tissue and human islets. Pancreases from cadaveric organ donors with diabetes mellitus were excluded from the studies apart from one organ donor with a history of type 1 diabetes.

Expansion of human adult and fetal pancreatic organoids

Human adult pancreatic organoids

Small clumps of adult human pancreatic exocrine tissue were obtained by mechanical dissociation of the islet-depleted tissue with a glass pipette. These clumps were plated in 24-well plates (Costar) at a density of ~15-20 clumps in a 30-40 µl drop of Matrigel (Basement membrane Growth Factor Reduced; BD Biosciences) as previously described (Sato et al., 2011). We next added 'Expansion Medium' (450µl/well), consisting of Advanced DMEM/F12 (Invitrogen) supplemented with 10 mM HEPES (Invitrogen), 1x Glutamax (Invitrogen), 1% penicillin/streptomycin (Sigma): B27 supplement (Invitrogen), N-2 supplement (Invitrogen), 1,25 µM N-acetylcysteine (Sigma), 50ng/ml EGF (Peprotech), 10 nM Gastrin (Tocris), 100 ng/ml FGF10 (Peprotech), 10% R-spondin1 conditioned medium (prepared in house), 100 ng/ml Noggin (Peprotech) or 10% Noggin conditioned medium (prepared in house), 500nM TGFβ inhibitor (A83-01; Stemgent). This Epidermal Growth Factor/Noggin/R-spondin (ENR)-based medium was adapted from Sato et al. (Sato et al., 2009). Passages were performed each 7 to 14 days. During passaging the organoids were

retrieved from the Matrigel with ice-cold Advanced DMEM/F12, mechanically dissociated into small pieces and transferred to fresh Matrigel in a 1:4 split ratio. The expansion culture medium was refreshed every 2-3 days. Cryopreservation of adult pancreatic tissue was done directly in CryoStem™ Freezing Medium (Stemgent). CoolCell^{R} freezing containers (Biocision) were used to allow for controlled freezing of the tissue to -80ºC. Cells were stored in liquid nitrogen.

Human fetal pancreatic organoids

Fetal pancreas for organoid culture was either plated directly or cryopreserved at -80C in freezing medium (50% FCS, 50% DMSO). To prepare samples for seeding, cryopreserved fetal pancreas was first transferred from -80C to 3ml Advanced DMEM/F12 (Invitrogen) at 37C, and incubated for 10 min in an incubator, before repeating this twice in fresh medium. Defrosted cryopreserved samples or fresh fetal pancreas were then minced with a sterile razorblade to obtain small clumps of pancreatic tissue. Lastly, minced tissue was plated in Matrigel and cultured under similar conditions as adult pancreatic organoids. Samples for RNA-extraction were isolated, and stored at -80C for later analysis.

Growth curve of expansion organoids

Organoids were dissociated by trypsinisation with Tryple Express (Gibco) for 5 minutes to retrieve single cells. Cell numbers were counted with a Burker-Turk haemocytometer at the end of each passage. 5 wells were counted per time point and the mean number of cells per well was determined.

Expansion of organoids derived from dispersed single cells.

Human adult pancreatic organoids expanded for 7 days were dispersed by trypsinisation with Tryple Express (Gibco) for 5 minutes. Single cells were obtained by filtering the cell

suspension over a 40 µm cell strainer (Fisher scientific) and plated (1000 cells/well) in a drop of 50 µl Matrigel/well of a 24-well plate, and cultured with Expansion Medium (see above) supplemented with 10nM Rock inhibitor Y27632 (BioVision). Rock inhibitor enhances survival of dissociated cells in our organoid culture system, in line with published results for dissociated hESCs (Watanabe et al., 2007).

Aldefluor™ labelling and cell sorting

Labelling of progenitor cells in the organoids using the Aldefluor™ fluorescent reagent system (Stemcell) was performed according to the manufacturer's protocol. Organoids were exposed to the fluorescent reagent for 45-60 minutes. They were imaged (Leica AF7000) immediately in the presence of the Aldefluor assay buffer, which contains ABC transport inhibitors that prevent active efflux of the Aldefluor product. For FACS experiments, single cells were isolated as described above, labelled for 45 minutes with the fluorescent reagent, washed several times and collected in Aldefluor™ assay buffer. ABD FACSAria II was used for sorting $ALDH^{lo}$ and $ALDH^{hi}$ cell populations. 4-Diethylaminobenzaldehyde (DEAB; an ALDH enzyme inhibitor) was used to set $ALDH^{hi}$ and $ALDH^{lo}$ gates, according to the manufacturer's protocol. Standard sorting protocols were followed and first a cell size gate was set on FSC/SCC plots to remove debris, then FSC-W and SSC-W were plotted to enable doublet discrimination and third, a live cell gate was made using the live/dead marker (7-AAD).

Colony-forming unit assay

After labelling with Aldelfuor and FACS (as described above), single $ALDH^{lo}$ and $ALDH^{hi}$ cells were plated in a dilution series of 1000 cells/well to 1 cell/well in 5µL Matrigel (8 replica per dilution; n=4). Cells were then provided with Expansion Medium supplemented

with 10nM Rock inhibitor Y27632 (BioVision), and colony (organoid)-forming units were counted on day 7 of expansion.

In vitro differentiation of human pancreatic organoids

The differentiation culture medium consisted of serum-free Dulbecco's modified Eagle medium/F12 (Invitrogen) supplemented with 2g/l human albumin (CeAlb, Sanquin), Insulin-transferrin-selenite-X (100X) supplement (Gibco), used at 1:1000, 10 mM nicotinamide (Pharmacy Leiden University Medical Center) and 1% penicillin/streptomycin (Sigma) (Yatoh et al., 2007).

In vivo differentiation: transplantation under the kidney capsule

To assess further *in vivo* differentiation of human pancreatic organoids, transplantation experiments were performed in 8–12 week old male NOD.Cg-*Prkdc*^{scid} *Il2rg*^{tm1Wjl}/SzJ (NOD scid gamma, NSG) immunodeficient mice (Jax labs). Mice were cared for according to institutional guidelines of the Leiden University Medical Center or Hubrecht Institute. Transplantation of organoids was performed in normoglycemic or hyperglycemic mice under isofluorane anaesthesia. Hyperglycemia was induced less than 6 days before transplantation with a single dose of 130 mg/kg streptozotocin (Sigma). Blood glucose levels were measured three times a week using an Accu-Check Comfort Glucometer (Roche), and animals with blood glucose concentration >18 mM were considered hyperglycemic. Randomization for blood glucose levels was done just before transplantation, assuring similar levels for each donor (n=8) in both groups. Organoids were retrieved from the differentiation medium and washed with PBS several times before approximately 2.5 – 3.0 mm^3 of tissue (2.4-4.5x10^5 cells) was packed in a PE50 transplantation tube. The tissue was then carefully placed under the kidney capsule using a Hamilton syringe with a threaded plunger. Blood glucose levels of

hyperglycemic animals were measured 3 times a week. Grafted tissue and blood plasma samples were obtained 1 day or 1 month after transplantation. INS^+ cells within or closely associated with the $KRT19^+$ ductal structures were counted in the grafts. Animal experiments were approved by the institutional animal welfare committee.

Imaging and immunohistochemical staining

For immunohistochemical analysis, organoids were fixed in 4% paraformaldehyde (PFA) and embedded in paraffin. Tissue grafts under the kidney capsule were also fixed in 4% PFA overnight. Tissue sections (4 μm) were cut and incubated with primary antibodies at 4ºC overnight and with secondary antibodies at room temperature for at least 2 hours. Primary antibodies, their dilution, source and amplification strategies are listed in Supplemental Table S1.

Fluorescent images were captured with a Leica SP5 confocal/multiphoton microscope or with a PerkinElmer ultraview vox spinning disk microscope. Images were further processed with either LAS AF lite or Volocity software, respectively. Quantitative analyses were performed with image J (NIH, Bethesda). The proportion of immunostained cells out of DAPI-positive cells is presented. Brightfield pictures were captured with a Leica DMIL microscope and processed with Leica LAS AF lite software.

Quantitative-PCR (qPCR) and analysis

For qPCR gene expression analysis, total RNA was extracted using the RNeasy Mini Kit (Qiagen) or with Trizol extraction (Invitrogen). Complementary DNA (cDNA) was prepared by reverse transcription of 1 μg total RNA using 25 ng Oligo dT-primers (Invitrogen), 0.5 mM dNTP (Fermentas), M-MLV RT 5x buffer (Promega), 10mM dithiothreitol (Promega), 40 Units RNasin (Promega) and 200 Units M-MLV reverse transcriptase (Invitrogen). cDNA

was used for gene profiling.To determine quantitative gene expression levels, real time PCR was performed in the Icycler iQ Real-Time PCR Detection System (Bio-Rad). PCR reactions were set up with 40ng cDNA and ready-to-use reaction master mix (iQ SYBR green supermix, Biorad). Primers used are specified in Supplemental Table S2. Gene expression levels were determined as the average of three replicate wells, and levels were normalised to each of two internal controls GAPDH and B2M. B2M-normalised data are shown, and all statistically significant changes were confirmed with GAPDH normalisation.

RNA-sequencing and analysis

Samples for RNA extraction were re-suspended in RLT buffer (Qiagen), and extractions were carried out using the RNeasy Mini or Micro RNA Extraction Kit (Qiagen). For mRNA sequencing, 10ng of RNA per sample was processed using the CEL-Seq protocol (Hashimshony et al., 2012), and 75 bp paired end sequencing was carried out on an Illumina Nextseq. Next, Read 1 was aligned with the hg19 RefSeq human transcriptome (available from UCSC genome browser (Kent et al., 2002)) using Burrows-Wheeler Alignment (Li et al., 2010) with default parameters. Read 2 contained a barcode that identified the sample-of-origin for that read. The CEL-Seq method sequences only a short stretch of the 3′ end of a transcript, and yields one read per transcript. Reads-per-million (RPM) normalization was used per sample and only genes with more than 10 RPM in 4 or more samples were accepted for subsequent analysis. The total transcript count in each sample was first normalized to the median number of transcripts per sample. After normalisation of the samples, R was used to generate a correlation heatmap based on spearman correlations, and a principle component analysis was performed. The accession number for the RNA sequencing data reported in this paper is GEO: GSE108854.

smFISH

Organoids for single molecule FISH (smFISH) assessment were harvested and freed from Matrigel using Cell Recovery Solution (BD Biosciences), according to the manufacturer protocol, and subsequently washed and fixed in 4% formaldehyde, 30% sucrose PBS solution overnight. Next, fixed samples were transferred to optimal-cutting-temperature compound in a mold and frozen. Frozen samples were then sectioned, and processed for smFISH as previously described (Itzkovitz et al., 2011). Individual transcripts were imaged using previously described methods (Raj et al., 2008).

Human C-peptide measurements in mice

To assess insulin secretory function after organoid transplantation in immunodeficient mice, analysis of human C-peptide, which is secreted in a 1:1 molecular ratio with insulin from insulin producing cells, was performed. Blood was drawn from tail cuts of normoglycemic or hyperglycemic mice. In normoglycemic animals, an intraperitoneal glucose challenge (2 g/kg) was performed 45 minutes before blood withdrawal in order to stimulate insulin-producing cells. The blood was centrifuged and plasma kept at –20 ºC. Analysis of human C-peptide was performed using the human-specific ultra-sensitive C-peptide ELISA kit (Mercodia) according to the manufacturer's instructions.

Statistical Analysis

Values are shown as mean ± standard error of the mean (SEM). The Mann-Whitney U test was used as a non-parametric test. *P* values <0.05 were considered significant. Statistical software comprised SPSS and GraphPad Prism. Power calculations for animal studies were based on the expected variations from the experiments in NSG mice and based on previous

experience with human pancreatic tissue grafts. All animals that survived and where grafts were found under the kidney capsule (92%) were included in the study. No blinding of investigators was done with animal studies and their analyses.

Reference List

Hashimshony, T., Wagner, F., Sher, N., and Yanai, I. (2012). CEL-Seq: single-cell RNA-Seq by multiplexed linear amplification. Cell Rep. *2*, 666-673.

Itzkovitz, S., Lyubimova, A., Blat, I.C., Maynard, M., van, E.J., Lees, J., Jacks, T., Clevers, H., and van, O.A. (2011). Single-molecule transcript counting of stem-cell markers in the mouse intestine. Nat. Cell Biol. *14*, 106-114.

Kent, W.J., Sugnet, C.W., Furey, T.S., Roskin, K.M., Pringle, T.H., Zahler, A.M., and Haussler, D. (2002). The human genome browser at UCSC. Genome Res. *12*, 996-1006.

Li, H. and Durbin, R. (2010). Fast and accurate long-read alignment with Burrows-Wheeler transform. Bioinformatics. *26*, 589-595.

Raj, A., van den Bogaard, P., Rifkin, S.A., van, O.A., and Tyagi, S. (2008). Imaging individual mRNA molecules using multiple singly labeled probes. Nat. Methods *5*, 877-879.

Sato, T., Stange, D.E., Ferrante, M., Vries, R.G., van Es, J.H., van den Brink, S., Van Houdt, W.J., Pronk, A., Van, G.J., Siersema, P.D. et al. (2011). Long-term expansion of epithelial organoids from human colon, adenoma, adenocarcinoma, and Barrett's epithelium. Gastroenterology *141*, 1762-1772.

Sato, T., Vries, R.G., Snippert, H.J., van de Wetering, M., Barker, N., Stange, D.E., van Es, J.H., Abo, A., Kujala, P., Peters, P.J. et al. (2009). Single Lgr5 stem cells build crypt-villus structures in vitro without a mesenchymal niche. Nature *459*, 262-265.

Watanabe, K., Ueno, M., Kamiya, D., Nishiyama, A., Matsumura, M., Wataya, T., Takahashi, J.B., Nishikawa, S., Nishikawa, S., Muguruma, K. et al. (2007). A ROCK inhibitor permits survival of dissociated human embryonic stem cells. Nat. Biotechnol. *25*, 681-686.

Yatoh, S., Dodge, R., Akashi, T., Omer, A., Sharma, A., Weir, G.C., and Bonner-Weir, S. (2007). Differentiation of affinity-purified human pancreatic duct cells to beta-cells. Diabetes *56*, 1802-1809.